RSC Advances

ROYAL SOCIETY OF CHEMISTRY

www.rsc.org/advances

Synthesis, spectral characterization, structure studies, molecular docking and antimicrobial evaluation of new dioxidouranium(VI) complexes incorporating tetradentate N_2O_2 Schiff base ligands

S. Yousef Ebrahimipour[a,*], Iran Sheikhshoaie[a], Jesús Castro[b], Michal Dušek[c], Zeinab Tohidian[a, d], Václav Eigner[c], Moj Khaleghi [e]

[a] Department of Chemistry, Faculty of Science, Shahid Bahonar University of Kerman, Kerman, Iran.

[b] Departamento de Química Inorgánica, Universidade de Vigo, Facultade de Química, Edificio de Ciencias Experimentais, 36310 Vigo (Galicia), Spain.

[c] Institute of Physics ASCR, Na Slovance 2, 182 21 Prague, Czech Republic.

[d] Young Research Society, Shahid Bahonar University of Kerman, Kerman, Iran.

[e] Department of Biology, Faculty of Science, Shahid Bahonar University of Kerman, Kerman, Iran.

Corresponding author:

Dr. S. Yousef Ebrahimipour

Department of Chemistry, Faculty of Science

Shahid Bahonar University of Kerman

76169-14111, Kerman, Iran

Tel/fax: +98 34 3132 2143

E-mails addresses: Ebrahimipour@uk.ac.ir, Ebrahimipour@ymail.com

Abstract

Two new uranyl(VI) Schiff base complexes $[UO_2(L^1)(DMSO)]$ (**1**), where L^1= N,N′-di(5-bromosalicylidene)-1,2-cyclohexyldiaminate ligand and $[UO_2(L^2)(MeOH)]$ (**2**), where L^2= N,N′-di(5-bromosalicylidene)-*o*-phenylenediaminate ligand, were synthesized and characterized by elemental analysis, ^{1}HNMR, FTIR, UV-Vis, fluorescence spectroscopy and molar conductivity measurement. The structure of the H_2L^1 free ligand and both complexes (**1**) and (**2**) were also determined by single crystal X-ray diffraction. According to results obtained, the title complexes have distorted pentagonal bipyramidal geometry where positions around U(VI) centre are occupied by the ONNO donors of the deprotonated dibasic Schiff base ligands (L^1 for 1 and L^2 for (2)), two oxido groups and the oxygen of coordinated solvent. The antimicrobial activity of ligands and complexes was also screened against gram positive bacteria *Staphylococcus aureus* PTCC 1112, *Micrococcus luteus* PTCC 1110, *Bacillus cereus* PTCC 1015, *Enterococcus faecalis*; gram negative bacteria *Pseudomonas aeruginosa* PTCC 1214, *Escherichia coli* PTCC1330, *Pseudomonas sp*, *Klebsiella pneumoniae*); and fungus strain (*Candida albicans*). The molecular docking of GlcN-6-P synthase with the synthesized compounds was also performed. According to results, complex **2** displayed minimum binding energy and can be considered as a good antimicrobial agent.

Keywords: dioxidouranium(VI); Schiff base complex; X-ray crystallography, Antimicrobial activity

Introduction

Schiff base ligands are one of the famous families of chelating ligands [1]. They coordinate to a wide range of metal ions and form metal complexes with various oxidation states [2]. These compounds have diverse applications in different fields, including efficient catalysts [3, 4], antimicrobial and anticancer drugs [5, 6], sensors [7] magnetic properties [8], and non-linear optical applications [9].

Coordination chemistry of f-elements is rapidly developing because their complexes show unique luminescent and magnetic properties including relevance to luminescent systems with long lifetimes, photostability and line-like emission bands [10]. This makes complexes of f-elements useful for diagnostic tools in biological sciences. For example, these compounds have been used as markers for immunofluorescent assays or paramagnetic contrast agents in magnetic resonance imaging [11], and second-order nonlinear optical (NLO) chromophores [12]. Among f-elements, uranium is particularly interesting since it exhibits both heavy metal characteristics and radioactive properties [13].

Uranyl(VI) complexes play a central role in the development of coordination chemistry of actinides due to their high chemical stability and low radiological hazard [14]. Hence, they are applied in environmental field for reduction of nuclear waste generated from reactor fuel, and for the extraction of uranium from sea and soil [15]. Also, uranyl complexes have possible catalytic applications [16].

One of the most interesting properties of metal complexes is their antimicrobial activity [17]. Various methods have been reported to evaluate this activity. Glucosamine-6-phosphate synthase (GlcN-6-P synthase) has been recently considered as a new target in antimicrobial studies because GlcN-6-P produced by this enzyme is very crucial for the survival of the cell [18,19]. It has

been demonstrated that inactivation of GlcN-6-P synthase even for a short-time results in morphological changes, agglutination and lyses and so, is lethal for pathogenic microorganisms [20]. Therefore, each compound which interacts with the enzyme and inhibits its action can be proposed as an antimicrobial agent. Molecular docking is an efficient technique providing important information about the binding mechanism, affinity and activity of drug candidates to their protein targets such as GlcN-6-P synthase [21].

Herein, the tetradentate Schiff base ligands H_2L^1 and H_2L^2 and their dioxidouranium(VI) complexes were prepared and characterized using spectroscopic methods. Crystal structures of the synthesized compounds were also determined using single crystal X-ray diffraction. Furthermore antimicrobial activity of the synthesized compound was also evaluated against microorganisms.

Results and discussion

The reaction of H_2L^1 or H_2L^2 with equi-molar quantity of $UO_2(OAc)_2{\cdot}2H_2O$ in DMSO and methanol respectively gave the complexes $[UO_2(L^1)(DMSO)]$ and $[UO_2(L^2)(MeOH)]$. The synthesized complexes have orange red color. They are stable in air and soluble in most solvents except n-hexane and diethyl ether. The molar conductivities of the title complexes are in good agreement with their nonelectrolyte natures. The schematic diagram of the complexation process is shown in Fig 1.

FT-IR studies

Assignments of selected IR bands of the Schiff base ligands (H_2L^1), (H_2L^2) and their pentagonal bi-pyramidal U(VI) complexes are listed in the experimental section. Ligand H_2L^1 and its U(VI)

complex **1** show asymmetric vibration of CH_2 at 2921 and 2927 cm^{-1}, respectively. The absorption bands at 2852 cm^{-1} for H_2L^1 and at 2857 cm^{-1} for complex **1** corresponded to symmetric vibrations of CH_2. In the spectra of H_2L^1, the strong band at 1631 cm^{-1} is assigned to υ(C=N) while this characteristic band appeared at 1628 cm^{-1} in the spectrum of H_2L^2 [22, 23]. In the complexes these bands undergo a red shift indicating the coordination of the azomethinic nitrogens to the U(VI) ion . FT-IR spectrum of H_2L^1 revealed that this compound exists in *enol* form, while for the free ligand H_2L^2 , the bands at 2941 and 1734 cm^{-1} correspond to υ(NH) and υ(C=O), respectively [22], which shows the presence of H_2L in *enol-keto* form. Upon complexation, disappearances of these peaks prove that the H_2L^2 coordinates to the metal ion in the enolic form. Moreover, red shift of C-O band from 1367 and 1363 and cm^{-1} in H_2L^1 and H_2L^2 respectively, to 1349 for 1 and 1305 cm^{-1} for 2 supporting the phenolic oxygen take part in complexation.[24, 25] Dioxidouranium(VI) complex with a *trans*-UO_2 moiety exhibits two strong bands at 888 and 821 cm^{-1} in **1** and at 899 and 828 cm^{-1} in **2** assignable to υ_{asy}(*trans*-UO_2) and υ_{sy}(*trans*-UO_2), respectively. After coordination, the various vibrations of υ (U–O) and υ (U–N) are assigned to bands occurring at 484-431 cm^{-1} [26].

^{1}HNMR study

^{1}H NMR spectra of the synthesized compounds were recorded in DMSO-d_6 and is shown in Figs. S1-S4. For H_2L^1, the singlet signal at 13.3 ppm is attributed to O1H and O2H protons. In the spectrum of the ligand H_2L^2, the O1H and N1H signals appear at 12.9 and 10.9 ppm, respectively, indicating the presence of free ligand in *keto enol* form. The coordination of phenolic oxygen (*enolic* form) to U(VI) ion is confirmed by disappearance of these peaks in spectra of their complexes. In the ^{1}HNMR spectrum of H_2L^1, azomethine protons are revealed at

8.4 ppm that after complexation shift to downfiled and appeared at 9.3 ppm confirming the complextaion take place through methane nitrogen. In case of H_2L^2 the single signals at 10.1 and 8.9 ppm are associated to azomethinic protons. Appearance of two peaks for azomethin hydrogens is due to their different chemical environments in the structure of the ligand. In the spectrum of the complex 2, the azomethine proton signal is appeared at 9.6 ppm as a singlet signal, which confirms that azomethine nitrogen has been coordinated to the metal ion. In the ^{1}HNMR spectrum of complex **1**, CH_3 protons of coordinated solvent can be assigned at 2.43 ppm as single signal. The signals of CH_2 related to cyclohexane ring are appeared at 1.4-1.8 and 1.5-1.9 for H_2L and $[UO_2(L^1)(DMSO)]$, respectively. Proton resonance of CH in H_2L^1 disclosed at 3.3 ppm and in its U(VI) complex at 3.9 ppm. In the spectra of $[UO_2(L^2)(MeOH)]$, the signals at 4.1 ppm and 3.1 ppm are respectively corresponded to the protons of hydroxyl and methyl groups of the coordinated methanol. Finally, in the spectra of compounds, the protons of the aromatic rings are observed in the range of 6.6 -8.0 ppm.

Fluorescence properties

The fluorescence properties of the ligands H_2L^1, H_2L^2 and the complexes **1** and **2** were investigated at room temperature (298 K). H_2L^1 and H_2L^2 (10^{-3} M; EtOH solution) show an emission band at 498 and 476 nm, respectively, which are correlated to intraligand transitions. The fluorescence spectra of **1** and **2** (2×10^{-5} M; EtOH solution) are shown in Fig. S5. When excited at 350 nm, the emission band of **1** is located at 408 nm while for **2** it is observed at 376 nm. The observed emission bands of **1** and **2** show blue shift of 92–124 nm compared with that of its free ligand, which is due to the complexation. The fluorescent emission originates from

ligand to metal charge transfer (LMCT) occurring between the d^6 orbital of U(VI) and the chromophore ligand [27].

Electronic spectra

The electronic spectra were obtained in methanol at room temperature. In the UV-Vis spectrum of ligands, the intense bands at 225 nm for H_2L^1 and 244 nm for H_2L^2 are attributed to $\pi\rightarrow\pi^*$ transition of the aromatic rings and other bands are correlated to azomethine $\pi\rightarrow\pi^*$ and $n\rightarrow\pi^*$ transitions. These bands showed bathochromic shift in the electronic spectra of both complexes, indicating the coordination of ligand to the U(VI) ion. The bands 396 nm and 429 nm for **1** and 356 nm and 398 nm for **2** can be associated to charge transfer bands [26, 28]. The first CT band was assigned to electron transfer from 2p of nitrogen to 5f of the U(VI) and the second band, similar to other pentagonal bi-pyramidal U(VI) complexes, can be assigned to metal to ligand charge transfer and/or apical oxygen→ ($5f^0$) U(IV) transition which is allowed transition producing the orange red color. [26]

X-ray crystal structures

X-ray structure of H_2L^1

The ligand (R,R)-4,4'-dibromo-2,2'-[cyclohexane-1,2-diylbis(nitrilomethylidyne)]diphenol, H_2L^1, crystallized in the chiral monoclinic space group $P2_1$, and was found to be the same polymorph and enantiomer that was recently described [29]; and comparable with the orthorhombic form [30]. A view of the asymmetric unit is shown in Fig. 2, and representative distances and

angles are given in Table 1. There are two strong intramolecular O-H…N hydrogen bonds between the hydroxy O atom and the imino N atom, whose parameters are in Table 2.

The imine nitrogen atoms are implied in C-N-C angles of 118.9(3) and 117.0(3)º, and N-C-N angles of 121.8(4) and 119.4(3)º which are very close to the theoretical 120º for sp^2 hybridization for both atoms. The C=N distances of 1.277(5) and 1.295(6) Å correspond with a C=N double bond [31]. The dihedral angle between the benzene rings is 66.41(17)º, i.e. close to the value previously reported, 67.20(15)°. The cyclohexyl moiety is found with a chair ring conformation as demonstrated by Cremer & Pople puckering parameters of Q: 0.580(5) Å, θ: 177.4(5)º and φ: 36(12)º [32], and the nitrogen atoms bonded to the ring are both in equatorial position, in such a way that the angles between the C-N bond and the plane of the ring are 66.7(2) and 64.5(2)º.

The supramolecular packing is directed by several C-H...π interactions with the phenyl rings as is shown in Fig. 3 and 4. The parameters of these interactions are listed in Table 3. Fig. 3 shows how a chain parallel to the *c* axis is formed by two C-H...π interactions. Two new chains run parallel to this, and they are connected also through C-H...π interactions, as is shown in Fig. 4, generating a growing in the Miller plane ($\bar{1}$,1,0). Combination of both interactions creates a plane as can be seen in Fig. 5.

X-ray structure of $[UO_2(L^1)(DMSO)]$ (1)

In this structure, uranium(VI) is coordinated by two *trans* oxido groups, a tetradentate N,N′-di(5-bromosalicylidene)-1,2-cyclohexyldiaminate ligand (L^{2-}) and a DMSO molecule. Like in **2**, the $(L^1)^{2-}$ tetradentate ligand acts as trischelating dianionic ligand. There are six fused rings, two benzene ones, the cyclohexyl, two six-membered metallocycles and one five-membered metallocycle. The asymmetric unit contains two molecules with different orientation of the

DMSO ligand. One of the molecules with labelling scheme is shown in Fig. 6 while in Fig. 7 differences between the two molecules are highlighted. Table 4 contains selected bond lengths and angles for easy comparison with those of **2**.

The coordination sphere of the uranium atom is a distorted pentagonal bipyramid with the oxido ligands in apical positions. Apical U-O distances between 1.777(9) and 1.800(9) Å, and O–U–O angles of 178.1(4) and 178.8(3)º are in the same range that was found in **2**. The U–O(phenoxo) bond lengths range between 2.230(8) and 2.297(9) Å, only slightly shorter than in the salophen^{2-} compound. The U–O(DMSO) bond lengths are 2.383(9) and 2.377(8) Å for both molecules, slightly shorter to that found in [UO_2(salmnt)(DMSO)], 2.419(5) Å, [33] but similar to those found in the literature for other related complexes, for example between 2.375(9) and 2.381(6) Å in the DMSO uranyl compound derived from disalicylaldimine-N,N'-diphenylidene-propyl-thiosemicarbazones [34], and in other DMSO uranyl complexes. [35, 36]

Fig. 7 clearly shows the "book" conformation of the tetradentate N_2O_2 Schiff base ligand, with dihedral angle between the two salicylate rings of 61.2(6) and 66.0(6)º, i.e. more acute value that the one found in **2**, and even in the free ligand [33]. Like with the free ligand, the cyclohexyl moiety exhibits a chair ring conformation with puckering parameters for the two symmetry independent molecules evaluated as Q: 0.537(12), 0.577(13) Å; θ: 177.1(13), 173.4(13)º [32]. Again, carbon atoms bonded to the equatorial nitrogen are the R,R enantiomer.

The ligand L^1 is more flexible than L^2. This is probably the reason why the pentagonal coordination plane is almost planar, with a root mean square deviation of the best plane calculated for the five donor atoms of 0.037 and 0.123 Å respectively for the two independent molecules. The Uranium atom lies in the plane with negligible deviation 0.017 and 0.037 Å. The chelating angles in the pentagonal plane range from 64.8(3) and 64.4(3)º for the five-membered

chelate rings, between 69.9(3) and 71.1(3)º for the six-membered chelate rings, and between 75.2(3) and 79.7(3)º for those where the DMSO ligand is involved. Although the dispositions of these ligands are quite different in each molecule in the asymmetric unit, the value of these angles does not differ more than one degree. Note that the DMSO ligands are also implicated in weak non-classical hydrogen bonding interactions. In fact, the supramolecular structure is formed via non-classical hydrogen bonding interactions, and at least three of them imply the methyl groups of the DMSO ligand, as shown in Table 5 and Figs. 8 and 9. Also a very weak π–π interaction is found with distances between centroids of the two neighbour phenyl ring [symm. op. x+1, y, z] of 4.294(8) Å shown in Fig 10.

X-ray structure of $[UO_2(L^2)(MeOH)]$ (2)

$[UO_2(L^2)(MeOH)]$ consists of uranium(VI) coordinated by two *trans* oxido groups, a tetradentate N,N′-di(5-bromosalicylidene)-*o*-phenylenediaminate ligand $(L^2)^{2-}$ and a methanol molecule. The $(L^2)^{2-}$ tetradentate ligand acts as trischelating dianionic ligand. There are six fused rings, three benzene ones, two six-membered metallocycles and one five-membered metallocycle. An ellipsoid representation of the complex is shown in Fig. 11. The coordination sphere of the uranium atom is a distorted pentagonal bipyramid with the oxido ligands in apical positions. This geometry is usual for uranyl salophen^{2-} complexes, incorporating and additional ligand in the equatorial plane [37-39]. Apical U-O distances are 1.784(4) and 1.793(4) Å, not very different of values found in other seven-coordinated uranyl complexes (e.g., the complex with salicylaldehydehydrazone ligands [35] with U-O between 1.759(6) and 1.774(7) Å; a complex with thiodigycolate [40] with U-O between 1.751(7) and 1.779(7) Å; a complex with hepta-coordinated uranyl [37] with U-O 1.79 Å in average. They are, however, slightly shorter than those found in the

closely related complex (N,N'-bis(3,5-di-*t*-butylsalicylidene)-4,5-dimethyl-1,2-phenylenediamine)-(methanol)-dioxido-uranium(VI) [41] which has U-O bond lengths between 1.786(4) and 1.805(4) Å. The U–O(phenoxo) bond lengths are 2.330(4) and 2.246(4) Å, clearly shorter than the U–N(imine) bond lengths, 2.573(4) and 2.523(5) Å, and even the U–O(MeOH) bond length, 2.467(4) Å. As expected, all of them are longer than those in the apical position, since latter are formally double U=O bonds. These distances are comparable with those found in other Uranyl salophen^{2-} compounds [15, 33, 41]. The U-O(MeOH) bond distance is shorter to that found in the aforementioned related methanol complex (N,N'-bis(3,5-di-*t*-butylsalicylidene)-4,5-dimethyl-1,2-phenylenediamine)-(methanol)-dioxido-uranium(VI) [41] or in [2,2-(2,2-dimethylpropane-1,3-diyl)bis(azanylylidene)bis (methanylylidene) diphenolate]-(methanol)-dioxido-uranium(VI) [42], but an important hydrogen bond interaction is found in that complex, while it is absent in [$UO_2(L^2)$(MeOH)].

Tetradentate N_2O_2 Schiff base ligands, such as salophen^{2-}, are effective chelators and they are usually planar in their metal complexes because of the completely conjugated π-electron system. However, uranyl complexes behave differently and the dianionic salophen^{2-} ligand shows a severely bent conformation [15, 33, 41], with dihedral angle between the two salicylate rings of 70.2(3)º, and with dihedral angles to the central 1,2-diimine phenyl ring of 40.4(3) and 58.5(3)º, respectively. This "book" conformation is best viewed along the O-U bond of the coordinated MeOH because the "pages" are perpendicular to this bond (Fig. 12). The size of the uranyl moiety is considered the reason of the bending.

The pentagonal coordination plane of donor atoms is also distorted. The root mean square deviation of the best plane calculated for the five donor atoms is as high as 0.230 Å. The Uranium atom is located 0.015 Å from this calculated plane, and the most deviated atom from

this plane (0.326 Å) is the phenolic oxygen atom O1. When O1 is removed from these calculations, the rms deviation for the new plane calculated using the remaining four donor atoms is 0.023 Å, O1 is situated at 0.7941 Å from this plane and the uranium atom is 0.175 Å out of the plane. Other published uranyl salophen compounds [41] also show significant deviation of the pentagonal plane from the planarity with strongly deviated phenoxo oxygen.

The chelating angles in the pentagonal plane range from 63.7(2)º for the five-membered chelate ring, 70.4(2) and 70.0(2)º for the six-membered chelate ring, and 76.5(1) and 80.3(1)º for those where the MeOH is involved. The latter values are influenced by strong hydrogen bond (Table 6, Fig. 13) formed between the OH group of the MeOH and the phenoxy group of another molecule.

This interaction put limits on the position of MeOH. The structure also exhibits non–classical hydrogen bond C-H…O (Table 6) and a π,π-stacking interactions (Table 7) established between salicylidene and N,N'-phenylene rings, with distances between centroids 3.676(3) and 3.876(3) Å. These interactions cooperate to form chains of molecules along b (Fig. 14), while the above mentioned strong O-H…O hydrogen bond connects the chains into slabs extended along *bc* plane. Bromine is oriented to the space between the slabs (Fig. 15).

Antimicrobial activity

The antibacterial activity of compounds against 5 reference strains (*Pseudomonas aeruginosa* PTCC 1214, *Staphylococcus aureus* PTCC 1112, *Micrococcus luteus* PTCC 1110, *Bacillus cereus* PTCC 1015, *Escherichia coli* PTCC 1330), 3 clinical strains (*Pseudomonas sp, Klebsiella sp*, *Eterococcus faecalis*), and one yeast (*Candida albicans* PTCC 5027) were assessed by evaluating the presence of inhibition zone (IZ), MIC and MBC values. The results demonstrated

that all tested compounds are only effective against Gram positive bacteria and they have not antimicrobial effect against gram negative strains (Table 8) while ciprofloxacine, as a standard antibacterial agent showed no selectivity between gram- negative and –positive species. In addition, this antibiotic had no significant activity against clinical samples. We found that *Eterococcus faecalis* isolated from clinical samples were resistant to H_2L^2, $[UO_2(L)(DMSO)]$ and Ciprofloxacin antibiotic while it was sensitive to H_2L^1, $[UO_2(L)(MeOH)]$ and $UO_2(OAc)_2.4H_2O$. The MIC and MBC values for H_2L_2 and both U(VI) complexes were in the range of 30 mg/mL to 0.118 mg/mL (H_2L^1 was in range of 10 mg/mL to 39 µg/mL). The results of our study showed that the compounds were effective on gram positive bacteria and *C. albicans* PTCC 5027. It was observed that the compounds inhibited the growth of the microorganisms and killed them (Table 9). According the biofilm formation results, it was found that the chemical compounds repressed biofilm formation in some bacteria (Table 10). However they could not stop biofilm formation in *C. albicans* PTCC 5027 before minimum inhibitory concentration. Moreover, complexes 1 and 2 were compared with some similar U(VI) complexes previously synthesized [43] in terms of antimicrobial activity against S. aureus (gram positive), E. coli (gram negative) and C. albicans (fungi). According to the obtained results (Table 11), 1 and 2 show activity against S. aureus and C. albicans while 3, 4 and 5 are active against all three microorganisms. 6 and 7 are effective against C. albicans. Complex 8 shows activity only against E. coli.

Generally, complexation mostly improves the antimicrobial activity of a complex in comparison with its corresponding ligand which can be ascribed to: (i) increasing the lipophilicity of the complex compared with the ligand due to the delocalization of π-electrons over the whole chelate ring resulted in the enhancement of the penetration of the complex into the lipid membranes of

the microorganisms [44a] and (ii) influence of the complex on the respiration process of the microorganisms which in turn restricts further growth of the cell [44b]

Molecular docking

GlcN-6-P synthase was used as a target for antimicrobial activity of the synthesized compounds as potential inhibitors. The in silico active pocket prediction of amino acids of GlcN-6-P synthase involved in binding with the synthesized compounds, fluconazole and ciprofloxacine are presented in Fig. 16. Docking of fluconazole, ciprofloxacine and the molecules synthesized here with the enzyme showed that all of the inhibitors can bind to one or more amino acids in the active site. Theoretical binding affinity of the tested compounds was obtained in the range of -7.1 kcal/mol to -8.9 kcal/mol (Table 12). Among all docked molecules, complex **2** revealed the less binding energy in comparison with other docked molecules that suggesting it may be considered as a good inhibitor of GlcN-6-P synthase and subsequently a good antimicrobial agent. These data are in accordance with experimental results.

Conclusions

Two tetradentate Schiff base ligands H_2L^1, N,N′-di(5-bromosalicylidene)-1,2-cyclohexyldiamine and H_2L^2, N,N′-di(5-bromosalicylidene)-*o*-phenylenediamine, and their respective new uranyl(VI) Schiff base complexes $[UO_2(L^1)(DMSO)]$ and $[UO_2(L^2)(MeOH)]$ were synthesized and fully characterized using physicochemical and spectroscopic methods. X-ray structure analysis revealed that both complexes have distorted pentagonal bipyramidal geometry around uranium central atom where the metal ion chelated by donor atoms of deprotonated Schiff base ligand, two oxido group and oxygen atom of coordinated solvent. The antimicrobial activities of

the synthesized compounds were also investigated against microorganisms. Obtained results indicate that complex **2** and H_2L^1 have higher activity against selected bacteria and yeast. The docking studies gave the same results as those obtained by experimental investigations. According to *in silico* studies, among the all synthesized compounds and ciprofloxacine, complex **2** shows minimum binding energy and may be considered as good inhibitor of GlcN-6-P synthase that is accordance with experimental results.

Experimental

Chemicals and apparatus

All the chemical reagents used in experiments were of spectroscopic grade and used as received without further purification. Melting points were measured on an Electrothermal 9100 apparatus. Fourier transform infrared (FT-IR) spectra were recorded on a Schimadzu system FT-IR 8400 spectrophotometer using KBr pellets. Nuclear magnetic resonance spectra were recorded on Bruker Avance-400 MHz spectrometer using DMSO-d_6 as solvent and TMS as internal standard. Electronic spectra of the complexes were recorded at 4×10^{-5} mol L^{-1} in methanol using Cary 50 spectrophotometer in the range of 200–800 nm. Fluorescence experiments were carried out on a Cary Eclipse spectrofluorometer from 300 to 700 nm at room temperature.

Synthesis of Schiff base ligand H_2L^1 and H_2L^2

The Schiff base ligands H_2L^1 and H_2L^2 were synthesized as following procedure: 1 mmol of appropriate diamine (1, 2-Diaminocyclohexan or 1, 2-Diaminobenzene) were added to a 10-mL ethanolic solution of 5-bromo-2 hydroxy benzaldehyde (0.4 g, 2 mmol) and the reaction mixture

was stirred for ca. 15 min at room temperature. The formed precipitate was separated after filtration, washed with cold ethanol, and dried in desiccator over anhydrous $CaCl_2$.

N,N′-di(5-bromosalicylidene)-1,2-cyclohexyldiamine (H_2L^1)

Yield: 81%. m.p.: 165 °C. Anal. Calc. for $C_{20}H_{20}Br_2N_2O_2$ (480.19 g mol^{-1}): C, 50.02; H, 4.20; N, 5.83. Found: C, 50.03; H, 4.25; N, 5.89%. FT-IR (KBr), cm^{-1}: ν(OH) 3490, $\nu_{asy}(CH_2)$ 2921, $\nu_{sy}(CH_2)$ 2852, ν(C=N) 1631, $\nu(C=C_{ring})$ 1474, ν(C-O) 1367, δ_{oopb}(OH) 782, ν(CBr) 558.^{1}H-NMR (400 MHz, DMSO-d_6, 25 °C, ppm): δ = 13.3 (*s*, 2H; OH), 8.4 (*s*, 2H; CH=N), 6.7-7.6 (*m*, 6H, Ar-H), 3.3 (*s*, 2H, CH), 1.4-1.8 (*m*, 8H, CH_2). UV/Vis (MeOH) λ_{max}, nm (logε, L mol^{-1} cm-1): 225 (4.38), 260 (3.79), 341 (3.34)

N,N′-di(5-bromosalicylidene)-*o*-phenylenediamine (H_2L^2)

Yield: 85%. m.p.: 190 °C. Anal. Calc. for $C_{20}H_{14}Br_2N_2O_2$ (474.15 g mol^{-1}): C, 50.66; H, 2.98; N, 5.91. Found: C, 50.53; H, 2.90; N, 5.88%. FT-IR (KBr), cm^{-1}: ν(OH) 3629, ν(NH) 2941, ν(C=O) 1734, ν(C=N) 1628, $\nu(C=C_{ring})$ 1455, ν(C-O) 1363, δ_{oopb}(OH) 778, ν(CBr) 537.^{1}H-NMR (400 MHz, DMSO-d_6, 25 °C, ppm): δ = 12.9 (*s*, 1H; OH), 10.9 (*s*, 1H; NH), 10.1 (*s*, 1H; =CH-NH), 8.9 (*s*, 1H; CH=N), 6.6-7.9 (*m*, 10H, rings). UV/Vis (MeOH) λ_{max}, nm (logε, L mol^{-1} cm^{-1}): 244 (4.21), 275 (4.01), 345 (3.87).

Synthesis of dimethylsulphoxide- N,N′-di(5-bromosalicylidene)-1,2-cyclohexyldiaminate dioxidouranium(VI) [$UO_2(L^1)$(DMSO)] (1)

A reaction flask containing H_2L^1 (0.048 g, 0.1 mmol) in 7 mL DMSO was placed in an oil bath, then 0.1 mmol of $UO_2(OAc)_2{\cdot}2H_2O$ (0.04 g) was added to the mixture with constant stirring. The

mixture was refluxed for ca. 10 min. after cooling, the obtained dark orange precipitate was filtered off, and dried under vacuum over anhydrous $CaCl_2$.

Yield: 67%. m.p.: >300 °C. Anal. Calc. for $C_{22}H_{24}Br_2N_2O_2SU$ (826.34 g mol^{-1}): C, 33.95; H, 3.11; N, 3.60. Found: C, 33.93; H, 2.97; N, 3.68%. FT-IR (KBr), cm^{-1}: $\nu_{asy}(CH_2)$ 2927, $\nu_{sy}(CH_2)$ 2857, ν(C=N) 1616, $\nu(C=C_{ring})$ 1461, ν(C-O) 1349, ν $(S=O)_{DMSO}$ 963, ν_{asy}(*trans*-UO_2) 888, ν_{sy}(*trans*-UO_2) 821, ν (CSC) 636, ν(CBr) 536.^{1}H-NMR (400 MHz, DMSO-d_6, 25 °C, ppm): δ = 9.3 (*s*, 2H; =CH-NH), 6.9-7.8 (*m*, 6H, Ar-H), 3.9 (*s*, 2H, CH), 2.43 (*s*, 6H, S-CH_3), 1.5-1.9 (*m*, 8H, CH_2). UV/Vis (MeOH) λ_{max}, nm (logε, L mol^{-1} cm^{-1}): 233 (4.65), 243 (4.63), 356 (3.79), 398(3.51). Molar conductance (1×10^{-3} M, MeOH): 5 ohm^{-1} cm^2 mol^{-1}.

Synthesis of methanol- N,N'-phenylene-bis(5-bromosalicylideneaminato) dioxidouranium(VI) [$UO_2(L^2)$(MeOH)] (2)

A 5 mL methanolic solution of (H_2L^2) (0.047 g, 0.1 mmol) was added drop wise to a methanolic solution of $UO_2(OAc)_2{\cdot}2H_2O$ (0.04 g, 0.1 mmol) with constant stirring. The solution immediately turned to orange. The mixture was refluxed for 1 h. After cooling, the formed precipitate was collected by filtration, and washed successively with cold methanol, and dried under vacuum over anhydrous $CaCl_2$. Appropriate single crystals were obtained from the mother liquor with slow evaporation after 2 days.

Yield: 74%. m.p.: > 300°C. Anal. Calc. for $C_{21}H_{16}Br_2N_2O_5U$ (774.20 g mol^{-1}): C, 32.58; H, 2.08; N, 3.62. Found: C, 32.52; H, 2.01; N, 3.73%. FT-IR (KBr), cm^{-1}: ν(OH) 3388, ν(C=N) 1606, $\nu(C=C_{ring})$ 1455, ν(C-O) 1308, ν_{asy}(*trans*-UO_2) 899, ν_{sy}(*trans*-UO_2) 828, δ_{oopb}(OH) 751, ν(CBr) 541.^{1}H-NMR (400 MHz, DMSO-d_6, 25 °C, ppm): δ = 9.6 (*s*, 1H; CH=N), 6.9-8.0 (*m*, 10H, rings), 4.1 (*s*, 1H; OH), 3.1 (*s*, 3H; CH_3). UV/Vis (MeOH) λ_{max}, nm (logε, L mol^{-1} cm^{-1}): 252

(4.50), 308 (4.12), 354 (4.03), 396 (3.89), 429 (3.80). Molar conductance (1×10^{-3} M, MeOH): 9 ohm^{-1} cm^2 mol^{-1}.

Crystal structure determination

The X-ray single crystal diffraction was measured using the Gemini diffractometer of Oxford Diffraction controlled by CrysAlis Pro [45]. The radiation source was Mo-Kα produced by the classical sealed LFF tube, monochromated with the graphite monochromator and collimated by the Mo-Enhance fibre-optics collimator. For detection, we used the CCD detector Atlas. The samples H_2L^1 and **2** were twinned by twinning operation of 180° rotation about c* in H_2L^1 and about a* in **2**, resulting in partial overlaps in diffraction spots. In order to account for these overlaps, we used the hklf5 reflection file format where the overlaps were defined by the data reduction software Crysalis PRO. The sample **1** was a two domain crystal for which a reasonable twinning law could not be found. The samples **1** and **2** were moderately strong absorbers, but the analytical absorption correction based on crystal shape was used for all three samples.

The structures were solved by charge flipping software SUPERFLIP [46] and refined with Jana 2006 [47]. Hydrogen atoms were discernible in difference Fourier maps and could be refined to reasonable geometry. According to common practice, hydrogen atoms bonded to carbon atoms were kept in ideal positions with C-H = 0.96 Å. The hydrogen atoms attached to oxygen atoms were refined with restrained bond lengths. In both cases the U_{iso} was set to 1.2 U_{eq} of parent atom. In case of **1** and **2** only the heavy elements were refined with harmonic ADPs, since the harmonic ADPs of the second period elements resulted in just negligible improvements in R values. Thus, for the second period elements isotropic refinement was sufficient for proper description of the electron density. In case of H_2L^1 all non-hydrogen elements were refined with

harmonic refinement. Structures H_2L^1 and **1** were non-centrosymmetric; therefore the Flack parameter was refined. In case of H_2L^1 we determined the Flack parameter in a separate calculation because input data in hklf5 refinement could not be used for direct refinement of Flack parameter. Details concerning collection and analysis are reported in Table 13.

Test strains and culture media

Strains of bacteria and yeast were obtained from PTCC (Persian Type Culture Collection, Tehran). Antimicrobial activity of compounds against 5 reference strains (*Pseudomonas aeruginosa* PTCC 1214, *Staphylococcus aureus* PTCC 1112*, Micrococcus luteus* PTCC 1110, *Bacillus cereus* PTCC 1015, *Escherichia coli* PTCC 1330), 3 clinical strains (*Pseudomonas sp, Klebsiella sp*, *Eterococcus faecalis*) , and one yeast (*Candida albicans* PTCC 5027) were studied. The species of bacteria were grown in Mueller Hinton Agar/Broth (Merck). Brain Heart Infution Agar/Broth (Merck) was used for culturing of *Eterococcus faecalis*. *Candida albicans* PTCC 5027 was grown in Sabouraud Dextrose Agar/Broth (Merck). The concentrations of microbial suspensions were adjusted to 10^8cells/mL.

Antibacterial assay

The agar well diffusion method, described by Irshad et al. was used for the antimicrobial screening [48]. An overnight culture of each bacterium and yeast strains (18-24h) adjusted to a turbidity equivalent to a 0.5 McFarland standard [17]. The inoculums suspension of the microbial stains was swabbed on the entire surface of agar media. Wells were cut and 50 µl of the compound (30 mg/mL except H_2L^1=10 mg/mL) were added. The plates were incubated at 37°C for 24- 48 h. The antimicrobial activity was assayed by measuring the diameter of the inhibition

zone formed around the well. The diameter of the zone of inhibitions was measured by measuring scale in millimeter (mm). DMSO as solvent was used as a negative control whereas media with ciprofloxacin (standard antibiotic) and fluconazole (standard antifungal drug) were used as the positive controls. The experiments were performed in triplicate.

Determination of minimum inhibitory and bactericidal concentration

In order to determining of the minimal inhibitory concentration (MIC) and minimal bactericidal concentration (MBC) of the synthesized compounds, a broth microdilution method which previously described by Carson et al. was selected [49]. Using Mueller Hinton broth (Merck), series of twofold dilutions of the title compounds were performed in sterile 96 well microtiter plates. Serial dilutions ranging from 30 mg/mL to 0.118 mg/mL were prepared in medium except H_2L^1 that used Serial dilutions ranging from10 mg/mL to 39 µg/mL. 100 µL of each dilution were mixed with an equal volume of bacterial suspension. Positive and negative growth controls were prepared. The plates were incubated for 24h, at 37◦C, under normal atmospheric conditions. The MIC was defined as the lowest concentration (highest dilution) of the compounds that inhibited the visible growth (no turbidity), when compared to the control. Afterwards, 10µl of each well was transferred to Mueller Hinton agar plates and incubated for 24h, at 37◦C. The lowest concentration associated with no visible growth of bacteria on the agar plates was considered the MBC. All dilutions were performed in triplicate.

The biofilm formation assessment

In order to assay of anti-biofilm effect of the compounds, Microtiter plate adhesion assay was employed [50]. In this study, a culture of the bacteria and yeast were grown over night in the broth

media. Then, the overnight cultures were diluted 1:100 into fresh medium for biofilm assays. 100 µL of the dilution was added on well in a 96 well dish. For quantitative assays, we typically use 4-8 replicate wells for each treatment. The microtiter plate was incubated for 24 h, at 37°C. After incubation, 25 µl of 1% Crystal Violet was added to each well, shaking the plates three times to help the colorant to get the bottom of the well. After 15 minutes at room temperature, each well was washed with 200 µl sterile PBS to remove the planktonic cells and stain not adhered to the well. This process was repeated three times. Only the adhered bacteria forming the biofilm were kept on the surface of the well. The Crystal violet bound to the biofilm was extracted later with two washes of 200 µl of ethyl alcohol. The liquid washing alcohol was transferred to a glass tube containing 1.2 mL of alcohol and agitated. To determine the degree of biofilm formation, the absorbance was determined at 540 nm in an UV spectrophotometer. Controls were performed with Crystal Violet binding to the wells exposed only to the culture medium without bacteria. Data for biofilm formation of all strains were compared with the data for the negative control.

***In silico* studies**

The crystal structure of GlcN-6-P synthase was obtained from Protein Data Bank (http://www.pdb.org/pdb/home/home.do) with the PDB ID of 2VF5 at a resolution of 2.90 A° [51]. Binding site of the target was selected based on the amino acid residues involved in binding to glucosamine-6-phosphate of GlcN-6-P synthase as obtained from PDB with ID 2VF5 which would be considered as the best accurate active region solved by experimental crystallographic data. The coordination sphere of ciprofloxacine, as standard antimicrobial agent and the synthesized ligands and complexes were generated from their X-ray crystal structure as a CIF

file. Mercury software (http://www.ccdc.cam.ac.uk/) was then applied to convert the CIF files to PDB format. Finally, molecular docking studies were carried out using Autodock vina software [52] with the grid box size set at 27, 24, and 21 A for x , y and z, respectively, and the grid center set at 30.59, 15.822 and -3.497 for x , y and z, respectively. All molecular images and animations were produced using Discovery Studio Visualizer 4.5 package.

Supplementary data

CCDC 1031426, 1063191 and 1063192 contain the supplementary crystallographic data for $[UO_2(L)(MeOH)]$, H_2L^1 and $[UO_2(L')(DMSO)]$, respectively. A copy of this information may be obtained free of charge from The Director, CCDC, 12 Union Road, Cambridge, Cb2 1EZ, UK (fax: +44 1223 336 033); web page: http://www.ccdc.cam.ac.uk/cgibin/catreq.cgi

Acknowledgements

Authors gratefully acknowledge the financial support provided for this work by the Shahid Bahonar University of Kerman. Crystallography was supported by the project 14-03276S of the Czech science foundation.

References

1. E. J. Campbell and S. T. Nguyen, *Tetrahedron Lett.*, 2001, **42**, 1221-1225.
2. K. Nakajima, K. Kojima, M. Kojima and J. Fujita, *Bull. Chem. Soc. Jpn.*, 1990, **63**, 2620-2630.
3. M. Pooyan, A. Ghaffari, M. Behzad, H. Amiri Rudbari and G. Bruno, *J. Coord. Chem.*, 2013, **66**, 4255-4267.
4. R. Kumar, K. Mahiya and P. Mathur, *Dalton Trans.*, 2013, **42**, 8553-8557.
5. S. Y. Ebrahimipour, I. Sheikhshoaie, M. Mohamadi, S. Suarez, R. Baggio, M. Khaleghi, M. Torkzadeh-Mahani and A. Mostafavi, *Spectrochim. Acta, Part A*, 2015, **142**, 410-422.
6. P. K. Sasmal, R. Majumdar, R. R. Dighe and A. R. Chakravarty, *Dalton Trans.*, 2010, **39**, 7104-7113.

7. X.-M. Wang, R.-Q. Fan, P. Wang, L.-S. Qiang, Y.-L. Yang and Y.-L. Wang, *Inorg. Chem. Commun.*, 2015, **51**, 29-35.
8. D. Zhang, Z. Zhao, P. Wang and X. Chen, *J. Coord. Chem.*, 2012, **65**, 2549-2560.
9. C. R. Nayar and R. Ravikumar, *J. Coord. Chem.*, 2014, **67**, 1-16.
10. R. Krishnan, J. Thirumalai and A. Kathiravan, *Electron. Mater. Lett.*, 2015, **11**, 24-33.
11. N. Hildebrandt and H.-G. Lohmannsroben, *Curr. Chem. Biol.*, 2007, **1**, 167-186.
12. A. Valore, E. Cariati, S. Righetto, D. Roberto, F. Tessore, R. Ugo, I. L. Fragala, M. E. Fragala, G. Malandrino and F. De Angelis, *J. Am. Chem. Soc.*, 2010, **132**, 4966-4970.
13. Y. Zhang, I. Karatchevtseva, J. R. Price, I. Aharonovich, F. Kadi, G. R. Lumpkin and F. Li, *RSC Adv.*, 2015, **5**, 33249-33253.
14. L. R. Morss, N. M. Edelstein and J. Fuger, *The Chemistry of the Actinide and Transactinide Elements (Set Vol.1-6): Volumes 1-6*, Springer, 2010.
15. K. Takao and Y. Ikeda, *Inorg. Chem.*, 2007, **46**, 1550-1562.
16. J. L. Sessler, P. J. Melfi and G. D. Pantos, *Coord. Chem. Rev.*, 2006, **250**, 816-843.
17. S. Y. Ebrahimipour, I. Sheikhshoaie, A. Crochet, M. Khaleghi and K. M. Fromm, *J. Mol. Struct.*, 2014, **1072**, 267-276.
18. C. Bates and C. Pasternak, *Biochem. J*, 1965. **96,** 147-154.
19. H. Chmara, R. Andruszkiewicz, and E. Borowski, *Biochi. Biophys. Acta, 1986*. **870**(2), 357-366.
20. P. Shyma, B. Kalluraya, S. Peethambar, S. Telkar, and T. Arulmoli, *Eur. J. Med. Chem*., 2013. **68,** 394-404.
21. G. Jose, T. S. Kumara, G. Nagendrappa, H. Sowmya, J. P. Jasinski, S. P. Millikan, N. Chandrika, S. S. More, and B. Harish, *Eur. J. Med. Chem*., 2014. **77**, 288-297.
22. I. Sheikhshoaie, S. Y. Ebrahimipour, M. Sheikhshoaie, H. A. Rudbari, M. Khaleghi and G. Bruno, *Spectrochim. Acta, Part A*, 2014, **124**, 548-555.
23. S. Y. Ebrahimipour, M. Mohamadi, J. Castro, N. Mollania, H. A. Rudbari and A. Saccá, *J. Coord. Chem.*, 2015, **68**, 632-649.
24. S. Y. Ebrahimipour, H. Khabazadeh, J. Castro, I. Sheikhshoaie, A. Crochet and K. M. Fromm, *Inorg. Chim. Acta*, 2015, **427**, 52-61.
25. S. Y. Ebrahimipour, I. Sheikhshoaie, A. C. Kautz, M. Ameri, H. Pasban-Aliabadi, H. A. Rudbari, G. Bruno and C. Janiak, *Polyhedron*, 2015, **93**, 99-105.
26. a) A. Fasihizad, T. Barak, M. Ahmadi, M. Dusek and M. Pojarova, *J. Coord. Chem.*, 2014, **67**, 2160-2170; b) A. A. A. Emara and O. M. I. Adly, *Transit. Metal Chem*., 2007, **32**, 889-901.
27. S. K. Gupta, N. Sen and R. J. Butcher, *Polyhedron*, 2014, **71**, 34-41.
28. I. A. Cozaciuc, R. Postolachi, R. Gradinaru and A. Pui, *J. Coord. Chem.*, 2012, **65**, 2170-2181.
29. K. Ha, *Acta Crystallogr. Sect. Sect. E: Struct. Rep. Online*, 2012, **68**, o1449-o1449.
30. J. Yi and S. Hu, *Acta Crystallogr. Sect. Sect. E: Struct. Rep. Online*, 2009, **65**, 2643-2643.
31. F. H. Allen, O. Kennard, D. G. Watson, L. Brammer, A. G. Orpen and R. Taylor, *J. Chem. Soc., Perkin Trans. 2*, 1987, S1-S19.
32. D. T. Cremer and J. Pople, *J. Am. Chem. Soc.*, 1975, **97**, 1354-1358.
33. H. C. Hardwick, D. S. Royal, M. Helliwell, S. J. Pope, L. Ashton, R. Goodacre and C. A. Sharrad, *Dalton Trans.*, 2011, **40**, 5939-5952.

34. N. Özdemir, M. Şahin, T. Bal-Demirci and B. Ülküseven, *Polyhedron*, 2011, **30**, 515-521.
35. C. C. Gatto, E. S. Lang and U. Abram, *Inorg. Chem. Commun.*, 2003, **6**, 1001-1003.
36. R. Takjoo, S. W. Ng and E. R. Tiekink, *Acta Crystallogr. Sect. Sect. E: Struct. Rep. Online*, 2012, **68**, m244-m245.
37. T. Loiseau, I. Mihalcea, N. Henry and C. Volkringer, *Coord. Chem. Rev.*, 2014, **266**, 69-109.
38. G. Nocton, P. Horeglad, V. Vetere, J. Pécaut, L. Dubois, P. Maldivi, N. M. Edelstein and M. Mazzanti, *J. Am. Chem. Soc.*, 2009, **132**, 495-508.
39. K. P. Carter and C. L. Cahill, *Inorg. Chem. Front.*, 2015, **2**, 141-156.
40. D. K. Unruh, A. Libo, L. Streicher and T. Z. Forbes, *Polyhedron*, 2014, **73**, 110-117.
41. R. Kannappan, S. Tanase, D. M. Tooke, A. L. Spek, I. Mutikainen, U. Turpeinen and J. Reedijk, *Polyhedron*, 2004, **23**, 2285-2291.
42. M. Azam, S. I. Al-Resayes, G. Velmurugan, P. Venuvanalingam, J. Wagler and E. Kroke, *Dalton Trans.*, 2015, **44**, 568-577.
43. a) S. A. Sadeeka, M. S. El-Attara and S. M. Abd El-Hamid, *J. Mol. Struct*., 2013, **1051**, 30-40; b) M. Shebl and S. M. E. Khalil, *Montash. Chem*., 2015, **146**, 15-33; c) O. M. I. Adly, A. Taha and S. A. Fahmy, *J. Mol. Struct*., 2015, **1093**, 228-238; d) O. M. I. Adly, A. Taha and S. A. Fahmy, *J. Mol. Struct*., 2013, **1054-1055**, 239-250 ; e) O. M. I. Adly, A. Taha and S. A. Fahmy, *J. Mol. Struct*., 2015, **1083**, 450-459.
44. a) B. Shaabani, A. A. Khandar, H. Mobaiyen, N. Ramazani, S. S. Balula and L. Cunha-Silva, *Polyhedron*, 2014, **80**, 166–172; b) M. Imran, J. Iqbal, S. Iqbal and N. Ijaz, *Turk. J. Biol*. 2007, **31**, 67-72.
45. Agilent . CrysAlis PRO. Agilent Technologies, Oxfordshire, England, 2010.
46 L. Palatinus and G. Chapuis, *J. Appl. Crystallogr.*, 2007, **40**, 786-790.
47. V. Petříček, M. Dušek and L. Palatinus, *Z. Kristallogr.,* 2014, **229**, 345-352.
48. S. Irshad, M. Mahmood and F. Perveen, *Research J. Biol*, 2012, **2**, 1-8.
49. C. Carson, B. Cookson, H. Farrelly and T. Riley, *J. Antimicrob. Chemother.*, 1995, **35**, 421-424.
50. H. Kubota, S. Senda, N. Nomura, H. Tokuda and H. Uchiyama, *J. Biosci. Bioeng.*, 2008, **106**, 381-386
51. **S.** Mouilleron, M. A. Badet-Denisot, and B. Golinelli-Pimpaneau, *J. Mol. Biol*., 2008. 377(4), 1174-1185.
52. O. Trott and A. J. Olson, *J. Comput. Chem*., 2010, **31(2)**, 455-461.

Figure captions:

Fig. 1. Schematic diagram for complexatin process.

Fig. 2. ORTEP view of H_2L^1.

Fig. 3. Chain of H_2L^1 molecules connected by weak interactions along the *c* axis.

Fig. 4. Chain (top) and sheet (bottom) of H_2L^1 molecules. The sheet is parallel to the plane (-1,1,0).

Fig. 5. Sheet of H_2L^1 molecules parallel to the Miller plane (-1,1,0) view along the *a* axis.

Fig 6. Ortep view of one of the molecules (that with "A" labels) found in the asymmetric unit of $[UO_2(L^1)(DMSO)]$.

Fig. 7. View of the two molecules found in the asymmetric unit showed along the $U\text{-}O_{(DMSO)}$ vector.

Fig. 8. DMSO as donor for hydrogen bonds between two neighbor molecules of $[UO_2(L^1)(DMSO)]$.

Fig. 9. Other hydrogen bonds between molecules of $[UO_2(L^1)(DMSO)]$.

Fig. 10. π,π-stacking interactions in $[UO_2(L^1)(DMSO)]$.

Fig. 11. ORTEP view of $[UO_2(L^2)(MeOH)]$.

Fig. 12. "Book" conformation of $(L^2)^{2-}$. The compound is showed along the N(1), N(2), O(2) plane.

Fig. 13. Hydrogen bonds between two neighbor molecules of $[UO_2(L^2)(MeOH)]$.

Fig. 14. Chain of molecules of $[UO_2(L)(MeOH)]$ connected by weak interactions along the *b* axis.

Fig. 15. Slabs of molecules along bc plane, with bromine oriented to the space between the slabs.

Fig. 16. Docked H_2L^1, H_2L^2, $[UO_2(L^1)(DMSO)]$, $UO_2(L^2)(MeOH)]$, fluconazole and ciprofloxacine in the active pocket of GlcN-6-P. All images were generated using Discovery studio 4.5.

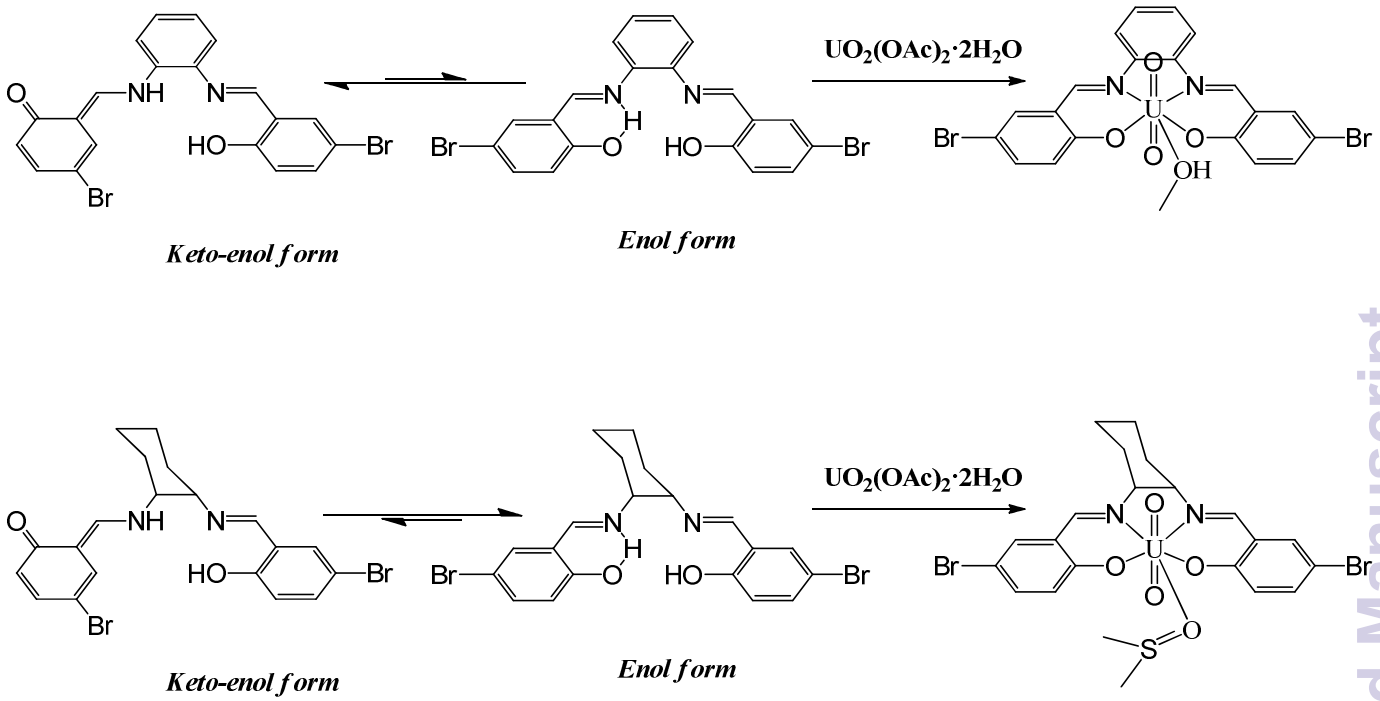

Fig. 1.

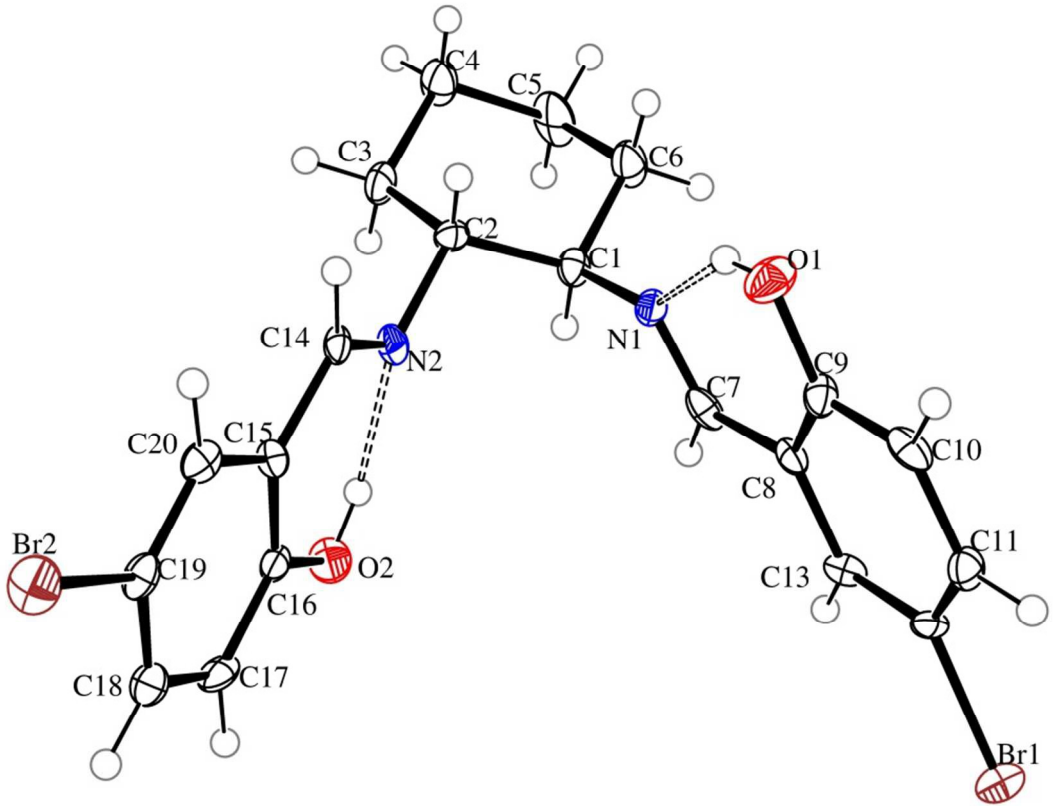

Fig. 2.

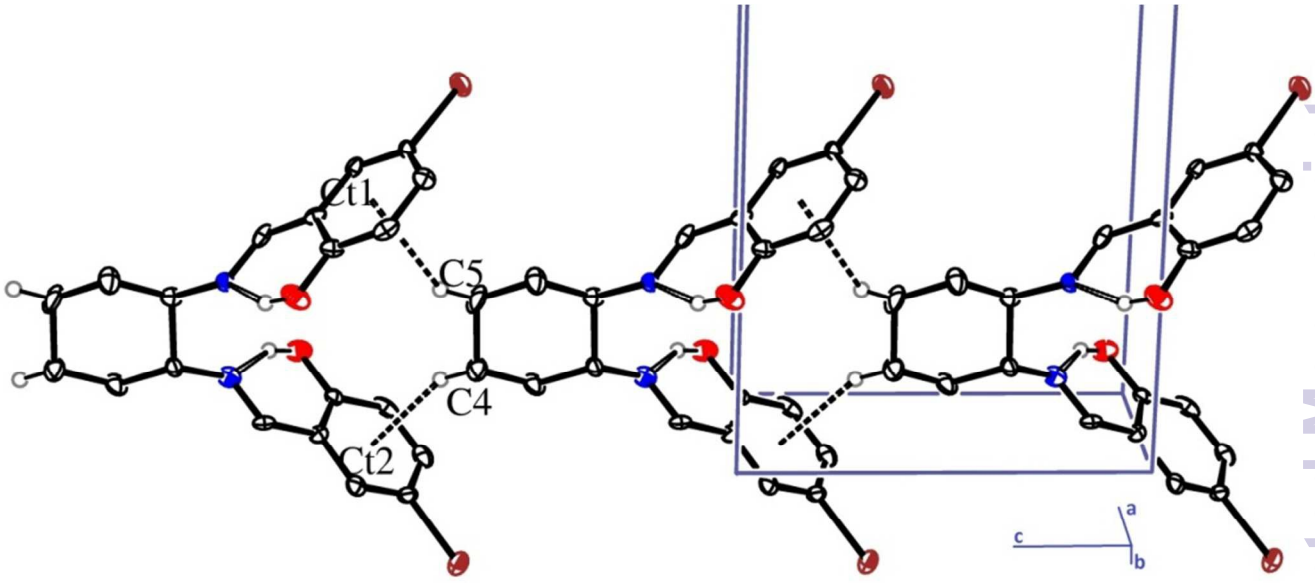

Fig. 3.

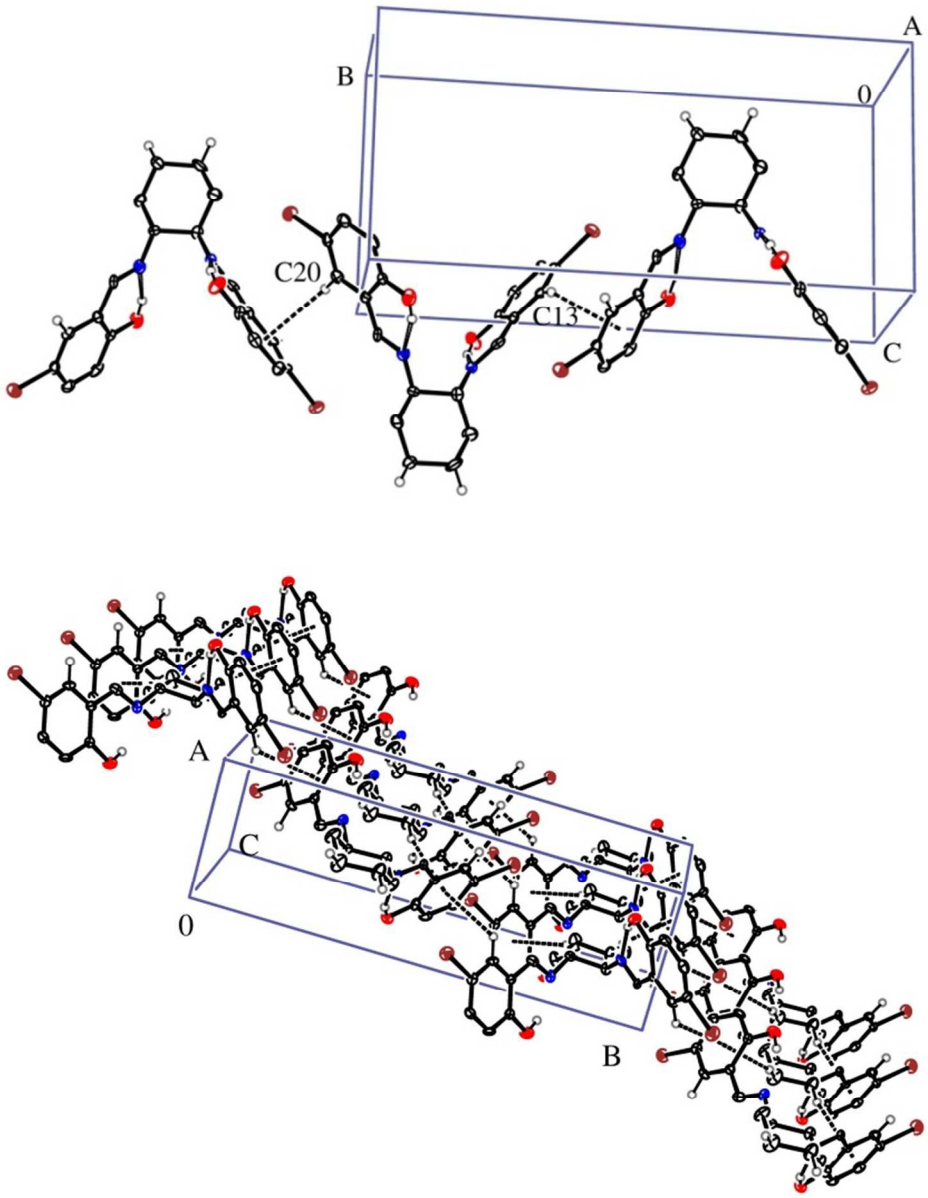

Fig. 4.

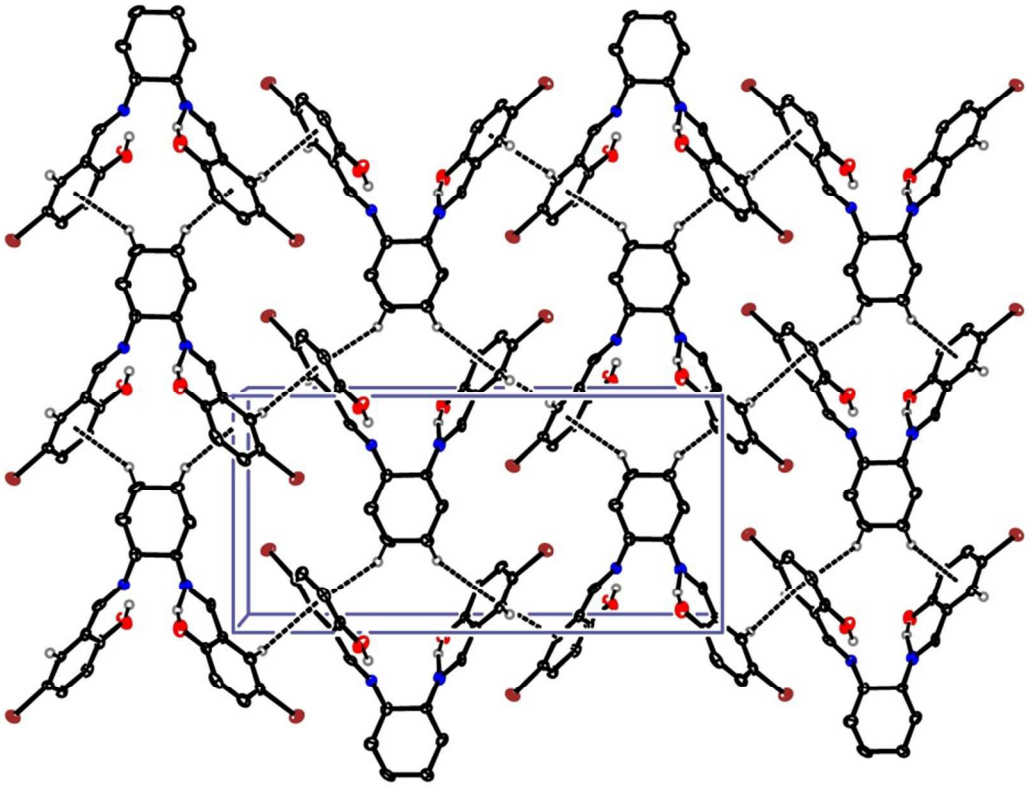

Fig. 5.

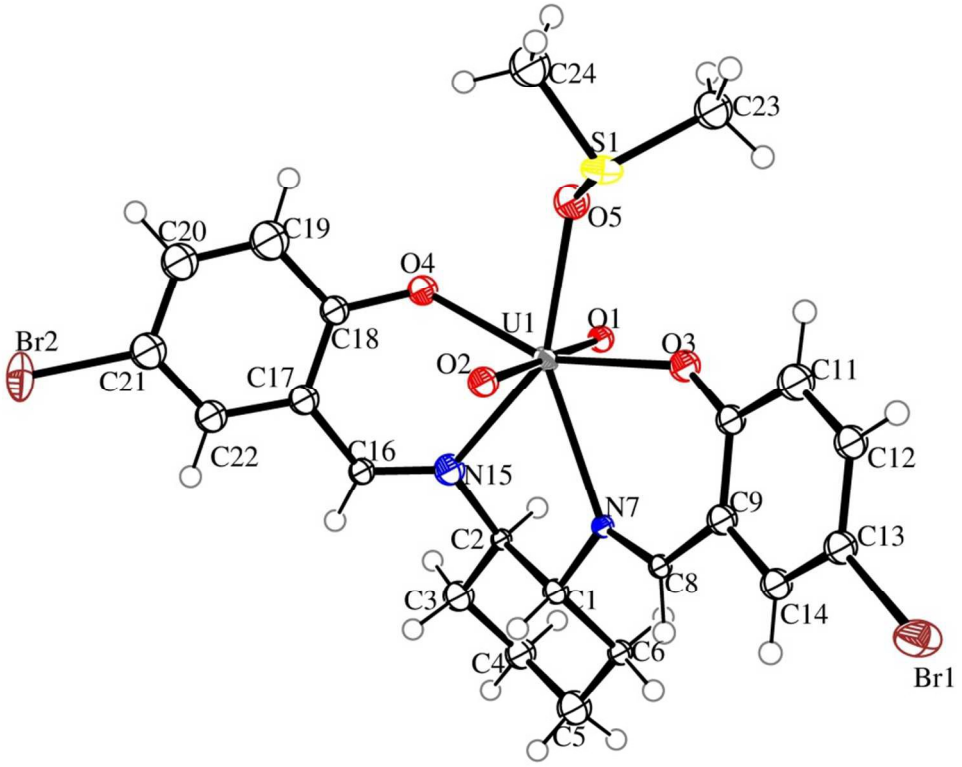

Fig. 6.

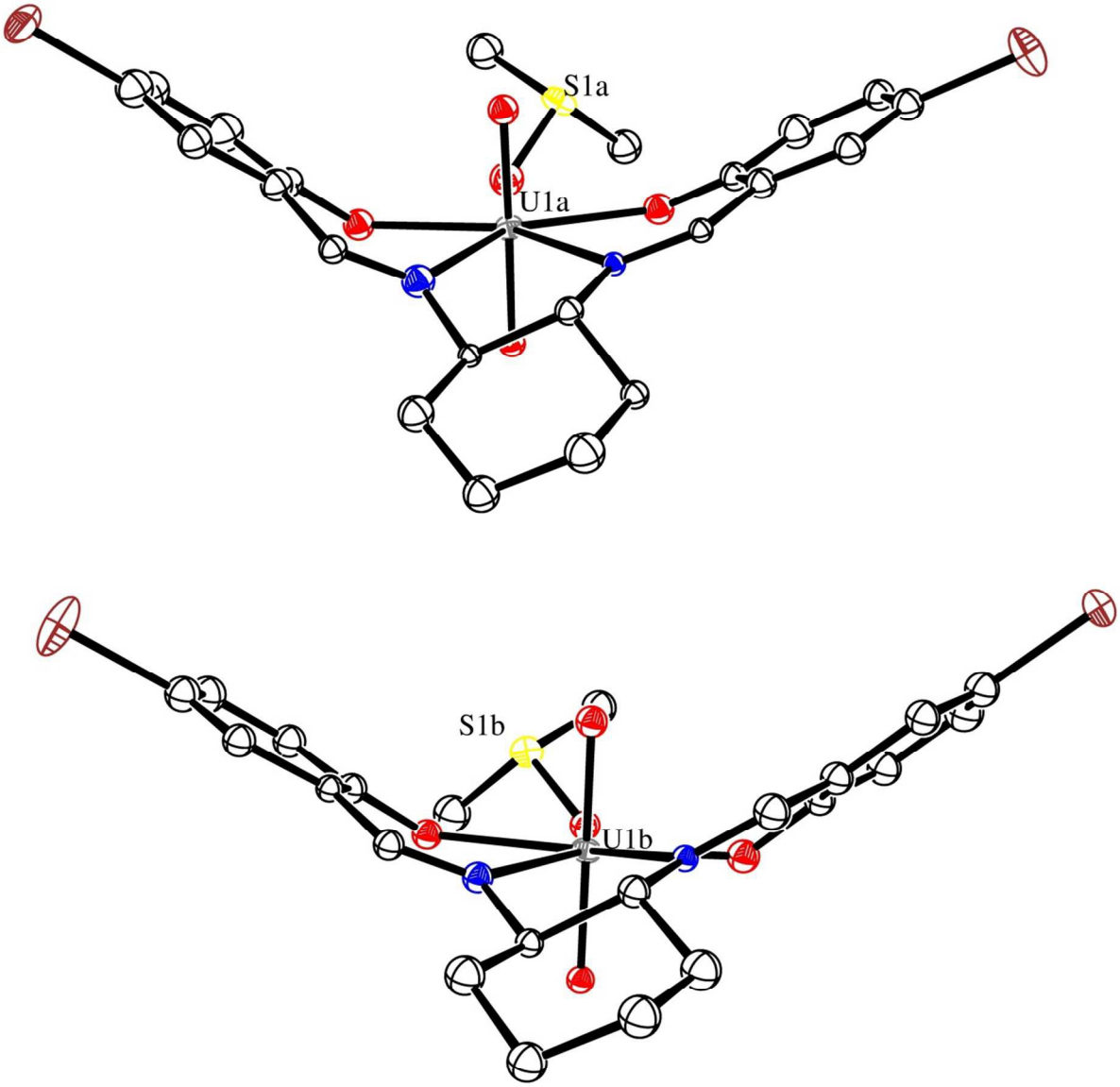

Fig. 7.

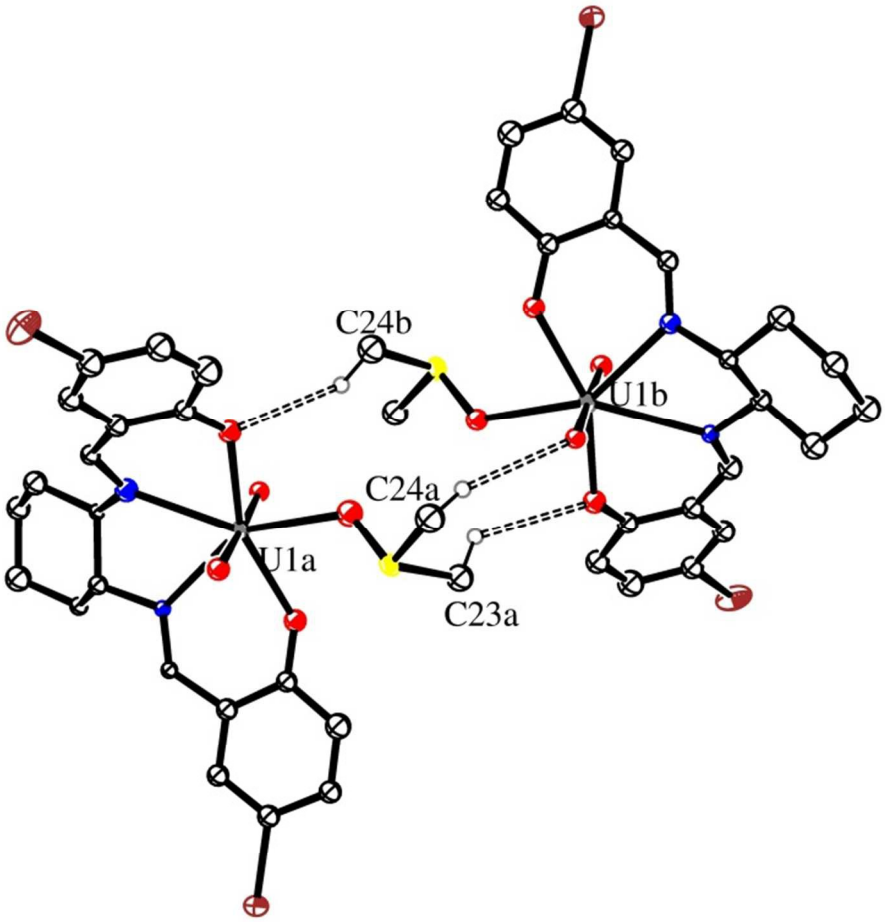

Fig. 8.

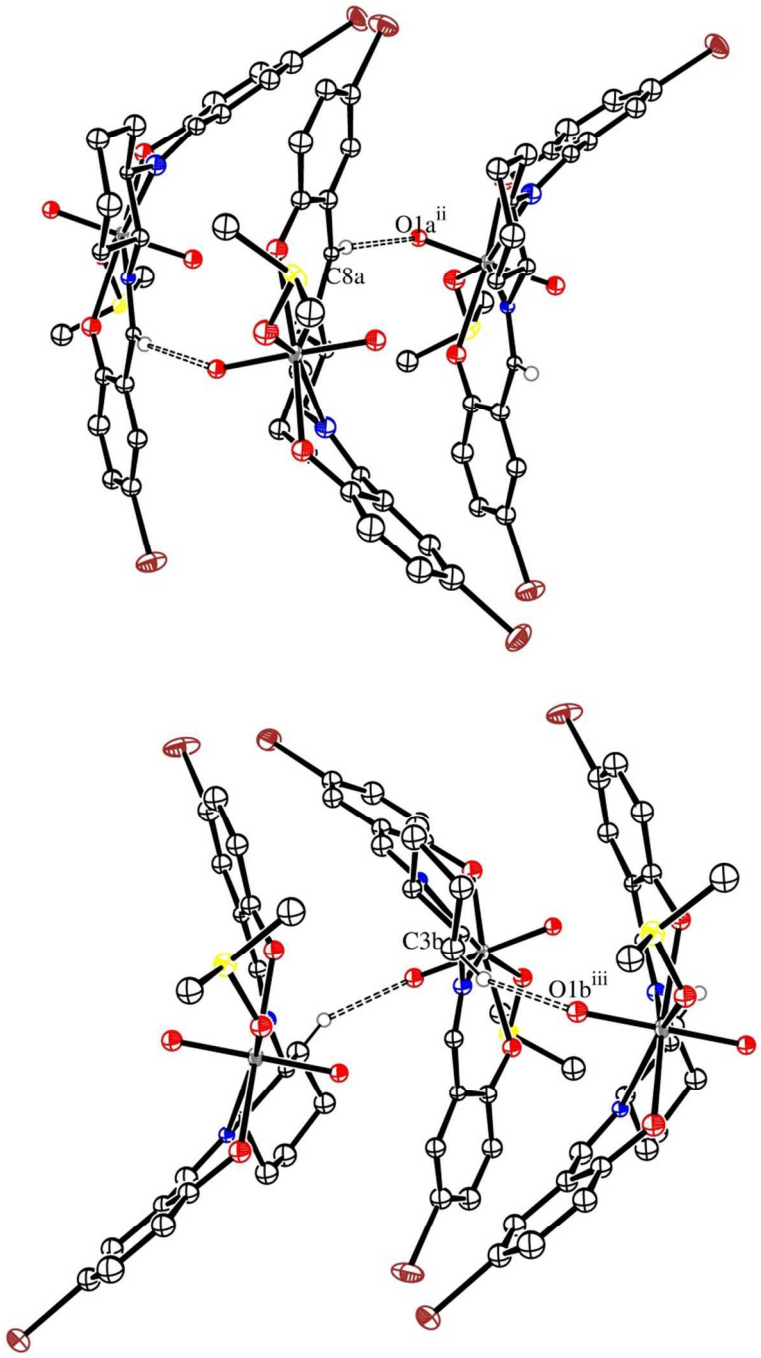

Fig. 9.

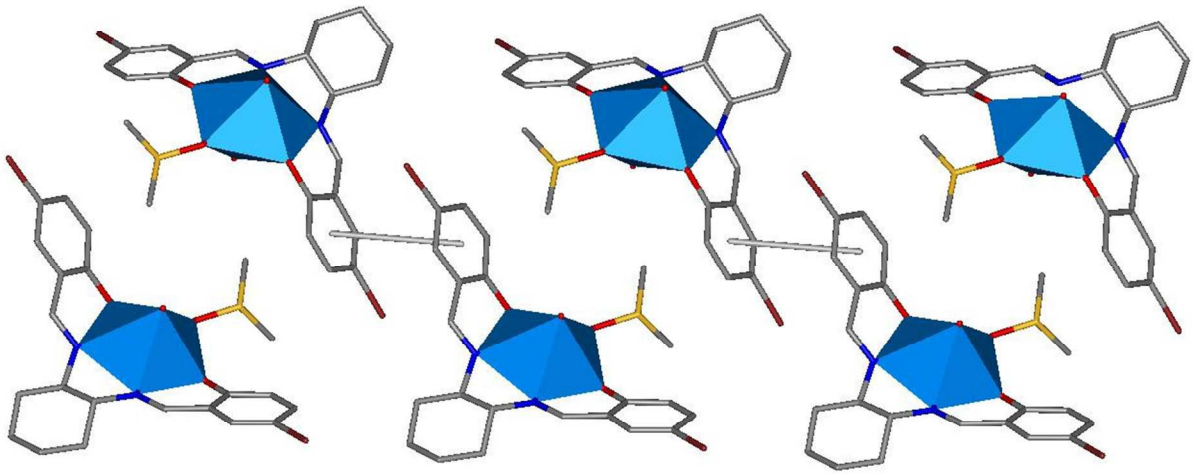

Fig. 10.

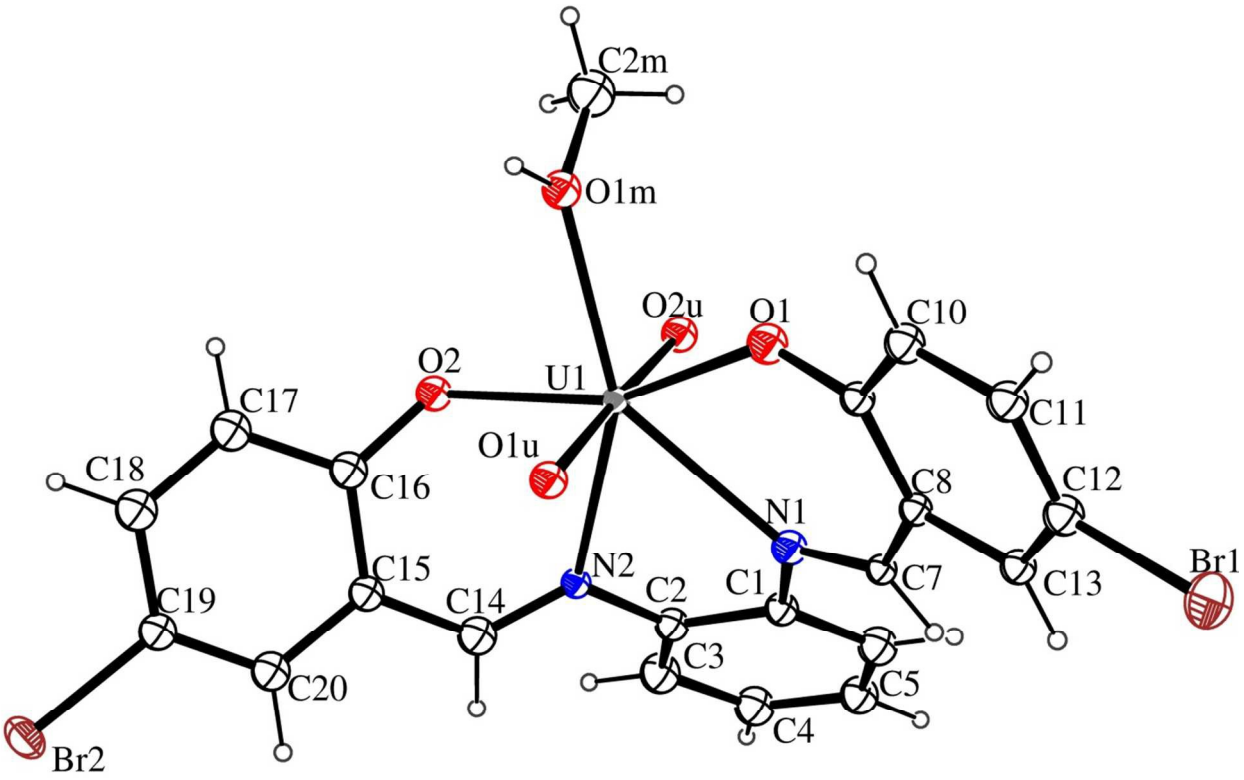

Fig. 11.

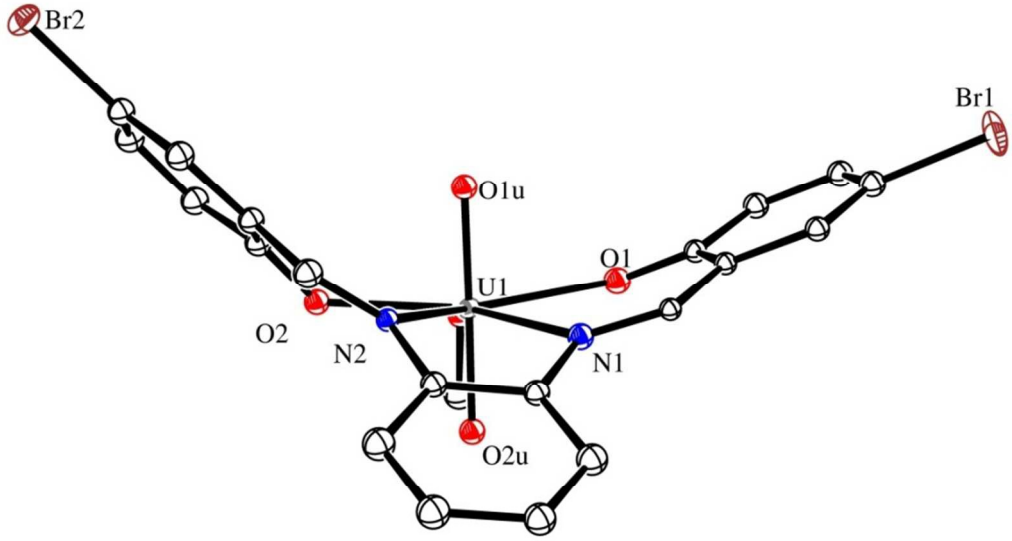

Fig. 12.

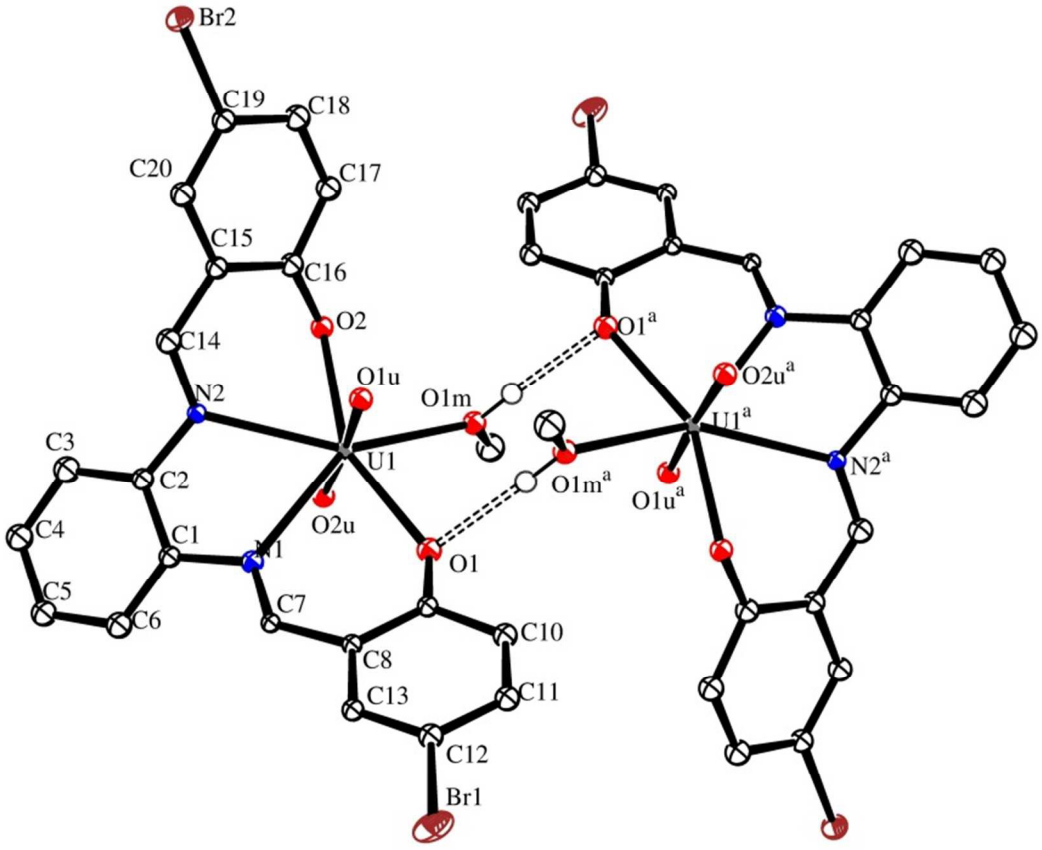

Fig. 13.

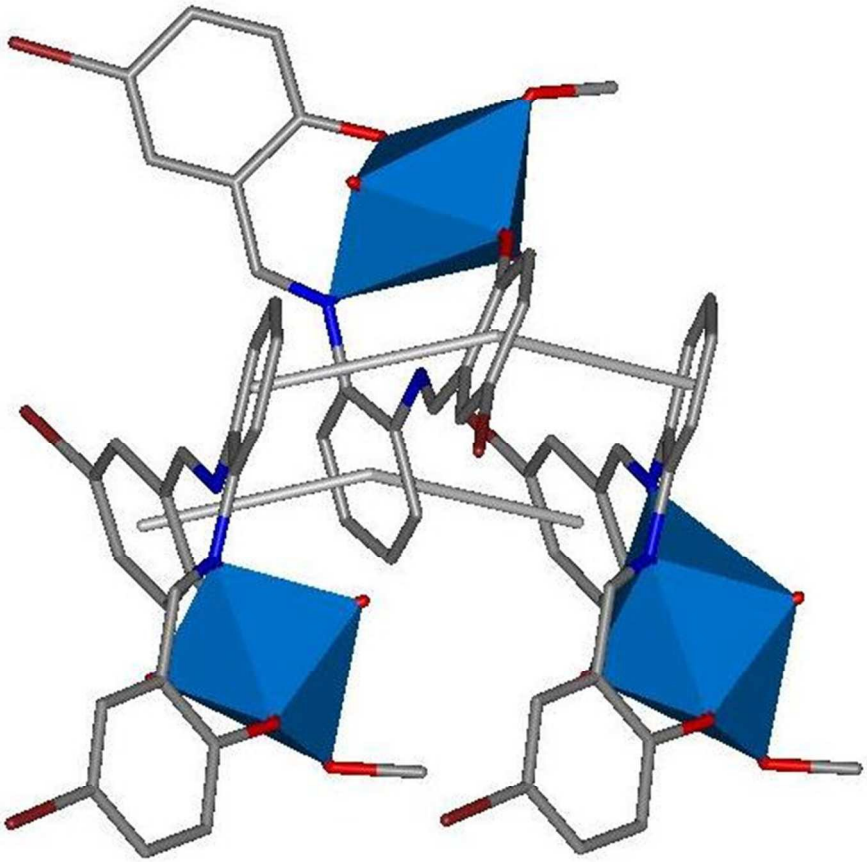

Fig. 14.

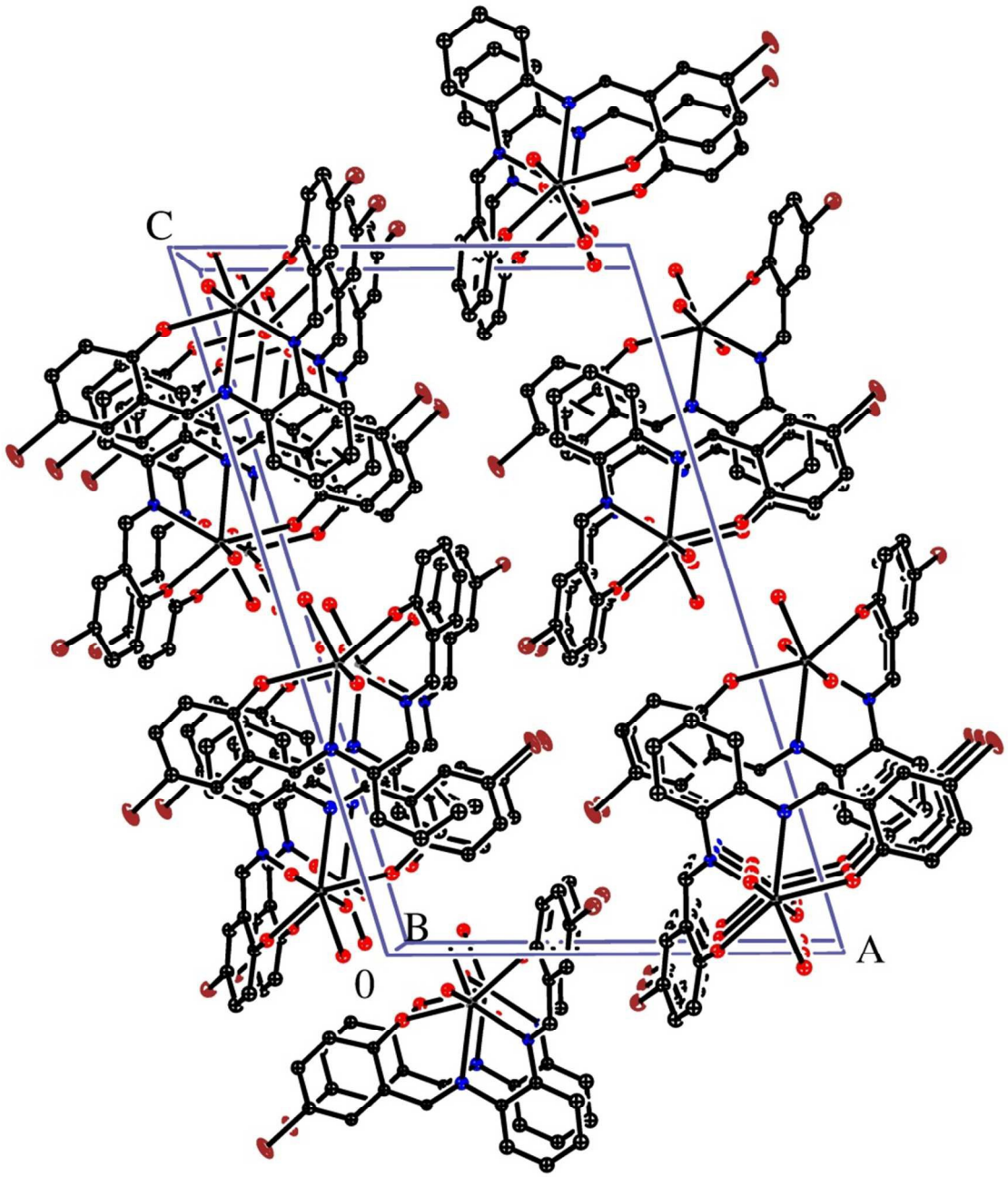

Fig. 15.

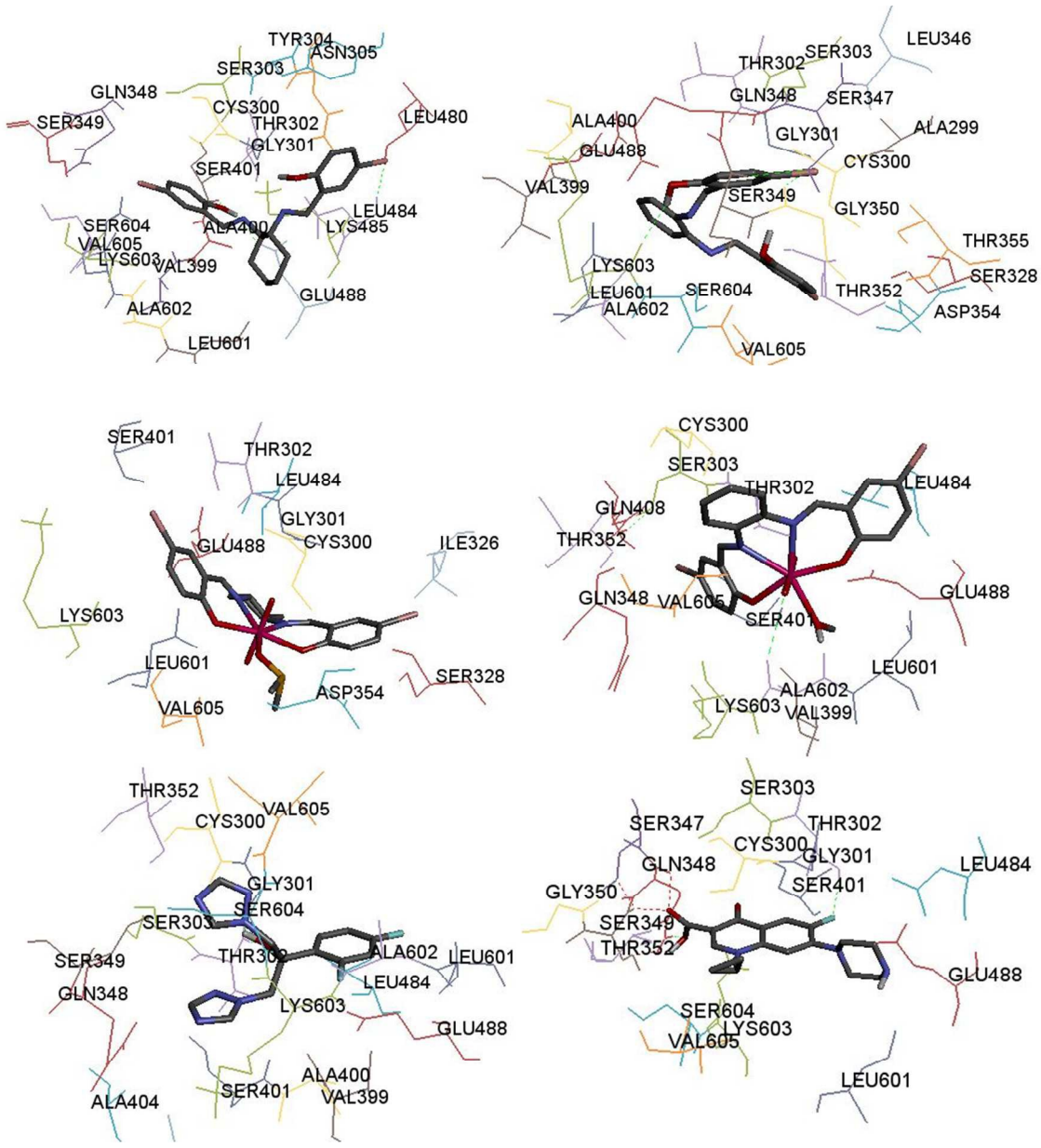

Fig. 16.

Table 1. Selected bond lengths [Å] and angles [°] and torsion angles [°] for H_2L^1.

O(1)-C(9)	1.360(5)	O(2)-C(16)	1.344(4)
N(1)-C(1)	1.471(5)	N(2)-C(2)	1.466(5)
N(1)-C(7)	1.295(6)	N(2)-C(14)	1.277(5)
Br(1)-C(12)	1.911(4)	Br(2)-C(19)	1.905(4)
C(1)-N(1)-C(7)	118.9(3)	C(2)-N(2)-C(14)	117.0(3)
N(1)-C(7)-C(8)	121.8(4)	N(2)-C(14)-C(15)	119.4(3)
N(1)-C(1)-C(2)	109.1(3)	N(2)-C(2)-C(1)	108.1(3)
N(1)-C(1)-C(6)	109.0(3)	N(2)-C(2)-C(3)	108.5(3)
C(1)-N(1)-C(7)-C(8)	177.5(4)	C(2)-N(2)-C(14)-C(15)	179.9(4)

Table 2. Hydrogen bonds parameters [Å and °] for H_2L^1.

D-H...A	d(D-H)	d(H...A)	d(D...A)	<(DHA)
O(1)-H(1O1)…N(1)	0.80(3)	1.92(3)	2.631(4)	147(3)
O(2)-H(1O2)…N(2)	0.85(3)	1.80(3)	2.579(4)	153(3)

Table 3. Summary of C-H···π interaction parameters for H_2L^1, [Å] and [°].

Interaction (*)	H..Cg [Å]	H-Perp [Å]	γ[°]	X-H..Cg	X..Cg[Å]	X-H···π
C4-H...Ct1[i]	2.80	-2.79	3.68	156	3.696(5)	64
C5-H...Ct2[i]	2.82	2.82	2.36	149	3.680(6)	61
C13-H...Ct1[ii]	2.90	2.85	10.40	125	3.536(4)	45
C20-H...Ct2[iii]	2.84	-2.82	6.82	132	3.561(4)	47

(*) Code: Symmetry operations: i: x, y, z+1; ii: 1-x, y-1/2 ,2-z; iii: -x, 1/2+y ,2-z; H-Perp, Perpendicular distance of H to ring plane; γ, Angle between Cg-H vector and ring normal; X-H···π, angle of the X-H bond with the π-plane

Table 4. Selected bond lengths[Å] and angles [°] for $[UO_2(L^2)(MeOH)]$ and $[UO_2(L^1)(DMSO)]$.

	$[UO_2(L^2)(MeOH)]$	$[UO_2(L^1)(DMSO)]$ Mol. A	$[UO_2(L^1)(DMSO)]$ Mol. B
U1-O1u	1.784(4)	1.779(9)	1.799(9)
U1-O2u	1.793(4)	1.777(9)	1.800(9)
U1-O1	2.330(4)	2.275(9)	2.297(9)
U1-O2	2.246(4)	2.235(7)	2.230(8)
U1-N1	2.573(4)	2.582(9)	2.587(9)
U1-N2	2.523(5)	2.499(10)	2.542(9)
U1-O1m(*)	2.467(4)	2.383(9)	2.377(8)
O1u-U1-O2u	176.56(19)	178.1(4)	178.8(3)
O1u-U1-O1	84.16(17)	91.4(3)	91.4(4)
O2u-U1-O1	97.60(17)	90.1(4)	89.0(3)
O1u-U1-O2	86.31(16)	89.5(3)	88.7(4)
O2u-U1-O2	93.35(17)	89.5(4)	91.5(3)
O1u-U1-N1	93.91(17)	91.8(3)	83.7(4)
O2u-U1-N1	83.86(17)	87.7(4)	95.3(3)
O1u-U1-N2	85.86(18)	87.8(3)	92.2(4)
O2u-U1-N2	90.79(18)	90.4(4)	86.7(3)
O1u-U1-O1m	99.72(16)	91.4(3)	89.6(4)
O2u-U1-O1m	83.59(17)	90.0(4)	91.6(3)
N1-U1-N2	63.68(16)	64.8(3)	64.4(3)
O1-U1-N1	71.99(16)	70.4(3)	71.1(3)
O1-U1-N2	133.63(15)	135.1(3)	134.6(3)
O2-U1-N1	133.93(16)	134.7(3)	133.7(3)
O2-U1-N2	70.41(15)	69.9(3)	70.5(3)
O1-U1-O1m	76.55(14)	76.0(3)	79.7(3)
O2-U1-O1m	80.31(14)	79.0(3)	75.2(3)
O1m-U1-N1	144.10(16)	146.2(3)	149.8(3)
O1m-U1-N2	149.82(15)	148.9(3)	145.6(3)
O1-U1-O2	153.04(15)	154.9(3)	154.9(3)

(*) O1m represents the oxygen donor atom of monodentated ligand, MeOH or DMSO. Other labels follows the $[UO_2(L)(MeOH)]$ scheme.

Table 5. Hydrogen bonds parameters [Å and °] for $[UO_2(L^1)(DMSO)]$.

D-H...A	d(D-H)	d(H...A)	d(D...A)	<(DHA)
C23A-H..O5B[i]	0.96	2.42	3.325(16)	156
C24A–H..O2B[i]	0.96	2.47	3.364(17)	154
C24B–H..O4A[ii]	0.96	2.57	3.428(17)	149
C3B–H..O1B[iii]	0.96	2.37	3.252(16)	152
C8A–H..O1A[iv]	0.96	2.38	3.273(13)	154

Symmetry transformations used to generate equivalent atoms:
i: x, 1+y, z; ii: x, y-1, z; iii, 1-x, y-1/2, 1-z; iv, 2-x, y-1/2, 2-z

Table 6. Hydrogen bonds parameters [Å and °] for $[UO_2(L^2)(MeOH)]$.

D-H...A	d(D-H)	d(H...A)	d(D...A)	<(DHA)
O1m-H..O1[i]	0.86(5)	1.94(4)	2.783(6)	164(6)
C7-H..O2u[a]	0.96	2.48	3.399(8)	160

Symmetry transformations used to generate equivalent atoms:
i: 2-x, -y, -z; a: 2-x,1/2+y, 1/2-z.

Table 7: π,π-stacking interaction parameters for $[UO_2(L^2)(MeOH)]$.

Centroids	Distance Ct-Ct(Å)	α	β	γ	Ct1-Perp (Å)	Ct2-Perp (Å)
Ct1-Ct2[a]	3.676(3)	8.4(3)	23.0	21.5	-3.421(2)	3.382(2)
Ct1-Ct2[b]	3.876(3)	8.4(3)	26.2	34.3	3.202(2)	-3.478(2)

Symmetry transformations used to generate equivalent atoms:
a = 2-x, 1/2+y, 1/2-z; b = 2-x, y-1/2, 1/2-z.

Table 8. In vitro antimicrobial activity of synthesized compounds (30 mg/mL) and H_2L^1 (10 mg/mL) by measurement inhibition zone diameter (mm).

Microorganism	Inhibition zone (mm)						
	H_2L^2	H_2L^1	**1**	**2**	$UO_2(OAc)_2.4H_2O$	Ciprofloxacin	Fluconazole
P. aeruginosa PTCC 1214	0	0	0	0	0	22	0
S. aureus PTCC 1112	10	0	8	21	9	25	0
M. luteus PTCC 1110	12	45	9	33	12	31	0
B. cereus PTCC 1015	9	15	0	22	9	24	0
E.coli PTCC1330	0	0	0	0	0	27	0
*Pseudomonas sp**	0	0	0	0	0	0	0
*Klebsiella sp**	0	0	0	0	0	0	0
*E. faecalis**	0	15	0	13	10	0	0
C. albicans PTCC 5027	0	13	8.5	19	7	0	35

* clinical bacteria

Table 9. Minimum inhibitory and lethal concentration of compounds. (MIC and MBC, mg/mL).

Microorganism	H_2l^2		H_2l^1		**1**		**2**		$UO_2(OAc)_2.4H_2O$	
	MIC	MBC	MIC	MBC	MIC	MBC	MIC	MBC	MIC	MBC
S. aureus PTCC 1112	0.465	0.938	-	-	7.5	15	3.75	15	1.875	7.5
M. luteus PTCC 1110	0.465	0.938	0.625	1.25	1.875	7.5	0.937	1.875	0.937	1.875
B. cereus PTCC 1015	1.875	-	1.25	2.5	-	-	0.937	1.875	1.875	7.5
*E. faecalis**	-	-	1.25	2.5	-	-	1.875	7.5	0.937	1.875
C. albicans PTCC 5027	-	-	2.5	5	1.875	7.5	7.5	15	15	30

* clinical bacteria

Table 10. Comparison of Anti-biofilm formation effect and MIC of compounds. (mg/mL)

Microorganism	H_2L^1		H_2L^2		**1**		**2**		$UO_2(OAc)_2.4H_2O$	
	ABF	MIC	ABF**	MIC	ABF	MIC	ABF	MIC	ABF	MIC
S. aureus PTCC 1112	-	-	0.235	0.465	1.875	7.5	0.937	3.75	0.937	1.875
M. luteus PTCC 1110	0.156	0.625	0.235	0.465	ND	1.875	0.469	0.937	0.469	0.937
B. cereus PTCC 1015	ND	1.25	ND***	1.875	-	-	ND	0.937	0.937	1.875
*E. faecalis**	0.625	1.25	-	-	-	-	0.937	1.875	0.235	0.937
C. albicans PTCC 5027	ND	2.5	-	-	ND	1.875	ND	7.5	ND	15

* clinical bacteria

** Anti-biofilm formation effect

*** Not Determined

Table 11. Comparison of the anti microbial activity of the complexes synthesized here with those reported in the literatura.

Compound	*Gram-positive*	*Gram-negative*	*Fungi*	*Ref.*
	S. aureus	*E.coli*	*C. albicans*	
$[UO_2(L^1)(DMSO)]$ (**1**)	●	○	●	Present work
$[UO_2(L^2)(MeOH)]$ (**2**)	●	○	●	Present work
$[UO_2(CIP\text{-}en)](OCH_3CO)_2.\ 6H_2O$/CIP-en (**3**)	●	●	●	43a
$[(L^1)UO_2]$ 2MeOH (**4**)	●	●	●	43b
$[(L^2)UO_2]\ 2H_2O$ (**5**)	●	●	●	43b
$[UO_2(L)(H_2O)_2]$ (**6**)	●	●	○	43c
$[UO_2(HL)(H_2O)(NO_3)]1.5H_2O$ (**7**)	●	●	○	43d
$[UO_2(L)]$ (**8**)	○	●	○	43e

Table 12: calculated binding affinity of synthesized compounds and standard drugs against GlcN-6-P synthase

Compound	Binding affinity (kcal/mol)	Compound	Binding affinity (kcal/mol)
H_2L^1	-7.8	Complex 2	-8.9
H_2L^2	-7.5	Fluconazole	-7.1
Complex 1	-7.4	Ciprofloxacin	-7.7

Table 13. Crystal data and structure refinement.

Compound	$[UO_2(L^2)(MeOH)]$ (**2**)	H_2L^1	$[UO_2(L^1)(DMSO)]$ (**1**)
Empirical formula	$C_{21}\ H_{16}\ Br_2\ N_2\ O_5\ U$	$C_{20}\ H_{20}\ Br_2\ N_2\ O_2$	$C_{22}\ H_{24}\ Br_2\ N_2\ O_5\ S\ U$
Formula weight	774.2	480.2	826.3
Temperature (K)	120	120	120
Wavelength (Å)	0.71073	0.71073	0.71073
Crystal system	Monoclinic	Monoclinic	Monoclinic
Space group	$P2_1/c$	$P2_1$	$P2_1$
Unit cell dimensions (Å, °)	a = 13.7720(6)	a = 5.8929(3)	a = 12.9681(6)
	b = 7.2047(3)	b = 18.6661(11)	b = 8.6124(4)
	c = 22.2442(9)	c = 9.0072(8)	c = 24.0605(10)
	β = 106.684(4)	β = 93.252(6)	β = 104.035(4)
Volume ($Å^3$)	2114.22(16)	989.17(12)	2607.0(2)
Z	4	2	4
$Density_{calc}$ (Mg/m^3)	2.4315	1.6117	2.1054
μ (mm^{-1})	11.494	4.121	9.406
F(000)	1432	480	1552
Crystal size (mm)	0.436 x 0.277 x 0.104	0.498 x 0.356 x 0.183	0.488 x 0.163 x 0.088
Θ range for data collection	2.98 to 29.27º	3.15 to 29.26º	2.87 to 29.37º
Reflections collected	9132	7584	22973
Independent reflections	9045	7557	12121
Reflections observed (>3σ)	7327	5769	9608
Θ Completeness at 98 % (°)	28.89	28.85	27.60
Absorption correction	Analytical	Analytical	Analytical
Max. and min. transmission	0.323 and 0.052	0.509 and 0.213	0.46 and 0.1
Data / restraints / parameters	9045 / 1 / 144	7557 / 3 / 242	12121 / 0 / 308
Goodness-of-fit on F^2	1.81	1.20	1.36
Final R indices [I>3σ(I)]	$R_1 = 0.0415$	$R_1 = 0.0306$	$R_1 = 0.0528$
	$wR_2 = 0.1087$	$wR_2 = 0.0765$	$wR_2 = 0.1211$
R indices (all data)	$R_1 = 0.0511$	$R_1 = 0.0453$	$R_1 = 0.0687$
	$wR_2 = 0.1131$	$wR_2 = 0.0814$	$wR_2 = 0.1340$
Flack parameter	no	0.03 (6)	0.29 (7)
$\Delta\rho_{max}$, $\Delta\rho_{min}$ ($e^-/Å^3$)	2.21, -2.34	0.57, -0.27	5.22, -4.25
CCDC number	1031426	1063191	1063192